ISSI Team, March 26, 2014

The Solar Wind – Atmospheric Electricity – Cloud Microphysics – Atmospheric Dynamics Connection: The Need to Clarify and Quantify the Links

Brian A. Tinsley
University of Texas at Dallas
tinsley@UTDallas.edu
http://www.utdallas.edu/physics/faculty/tinsley.html

OUTLINE

- Evidence for the electrical connection:

  Day-to-day timescale unique to electrical connection

  Dynamic responses to four independent space weather inputs, plus one tropospheric input , with only current density (J_z) in common

- Qualitative account of the connection:

  Global circuit models account for location and timing of responses

- Models needed: Charging of clouds

  Charging of layer clouds

  Charging of convective and cyclonic clouds

- Models needed: Electrical effects on cloud microphysics

  Five pathways to microphysical changes

- Models needed: Connection to global circulation

  To account for observed NAO and AO responses on day-to-day and inter-annual timescale, blocking, and storm track changes

☐ Summary and Conclusions

THE ELECTRICAL CONNECTION

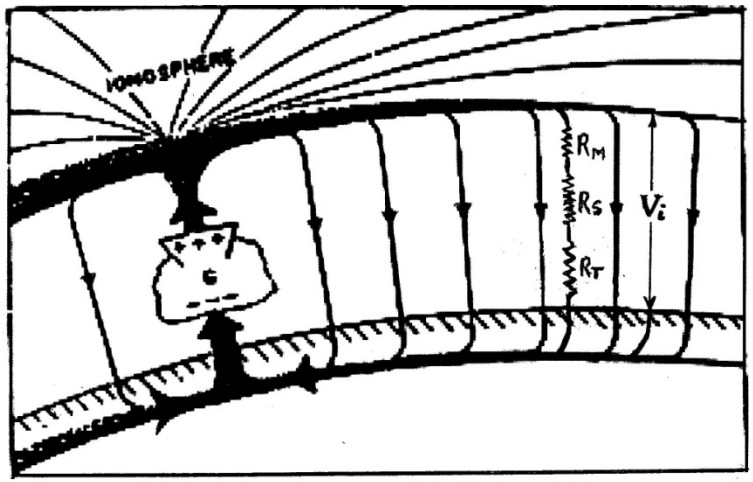

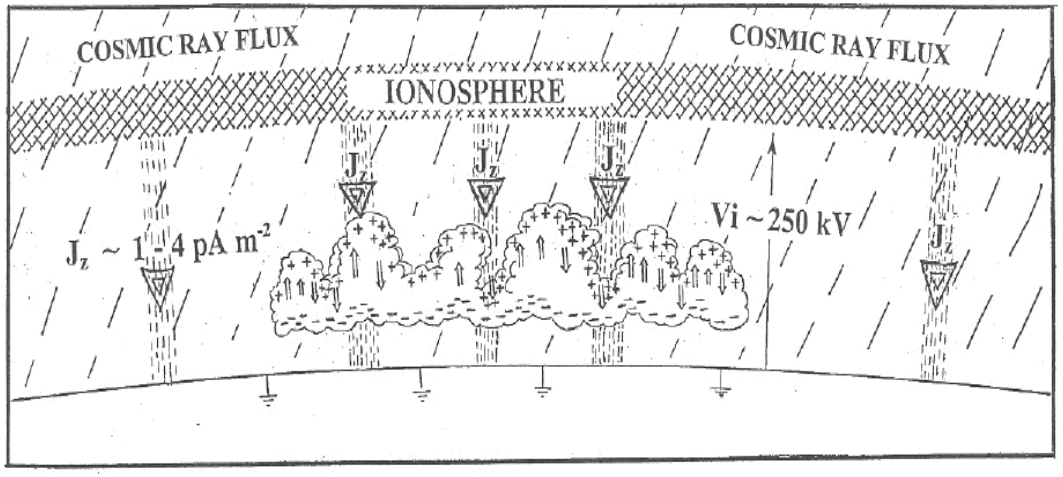

Each of about 1000 highly electrified storms around the globe sends about 1 Ampere to the Ionosphere , and it charges to ~ 250 kV.

The local downward current density, J_z, is given by Ohm's Law in three dimensions: $J_z = V_i / (R_M + R_S + R_T)$ where $R_M + R_S + R_T$ are the column resistances (Ω-m^2) of the mesosphere, stratosphere, and troposphere respectively. Any change in V_i, R_M, R_S, or R_T affects J_z.

R_M and R_S and R_T vary with cosmic ray flux, relativistic electron flux, and solar proton flux. V_i varies with IMF and solar wind speed changes.

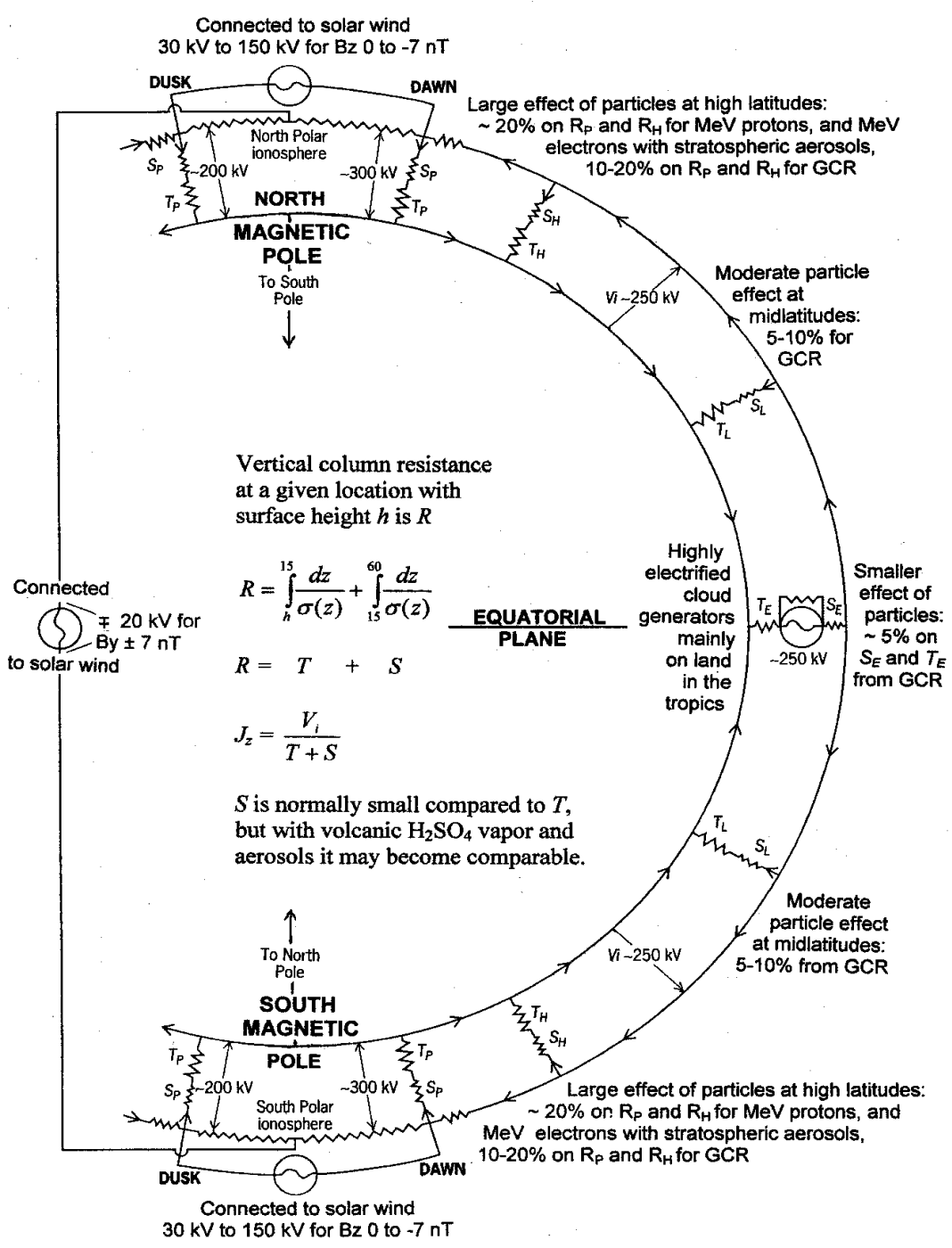

Schematic of a section through the global atmospheric electric circuit in the dawn-dusk magnetic meridian.

There are large changes (~20%) in column conductivities due to cosmic rays and other energetic space particle fluxes at high latitudes, and smaller changes (~ 5%) at low latitudes.

The solar wind produces changes in ionospheric potential of 10-20% at high latitudes.

Day-to-day global thunderstorm variations produce ~20% changes in global ionospheric potential.

All of these modulate the ionosphere-earth current density *Jz* that flows downward through clouds. From Tinsley, Rep. Prog. Phy., 71, 066801, 2008.

Evidence for the Electrical Connection

Timescales for responses as little as a few hours:

- The correlations are found on the day-to-day timescale
- J_z responds to changes in ionospheric potential or in column resistance in less than ten minutes
- J_z flows through clouds (they cover 70% of the globe) and it takes only a few hours for the microphysics to respond to J_z changes
- Chemical and dynamical changes in the stratosphere take more than a week to propagate down

Multiple inputs and responses with only J_z changes in common:

- Galactic cosmic ray flux strongly influence all of R_T, R_S, and R_M
- North-Solar wind electric field ($E_z = V_x x B_y$) superimposes on polar V_i
- Relativistic electron precipitation affects R_M and R_S with aerosols present
- Solar protons affect R_M and R_S with aerosols present
- Thundercloud generator V_i changes produce high latitude pressure changes the same as solar wind electric field V_i changes

From the analysis of Kirkland et al., 1996.

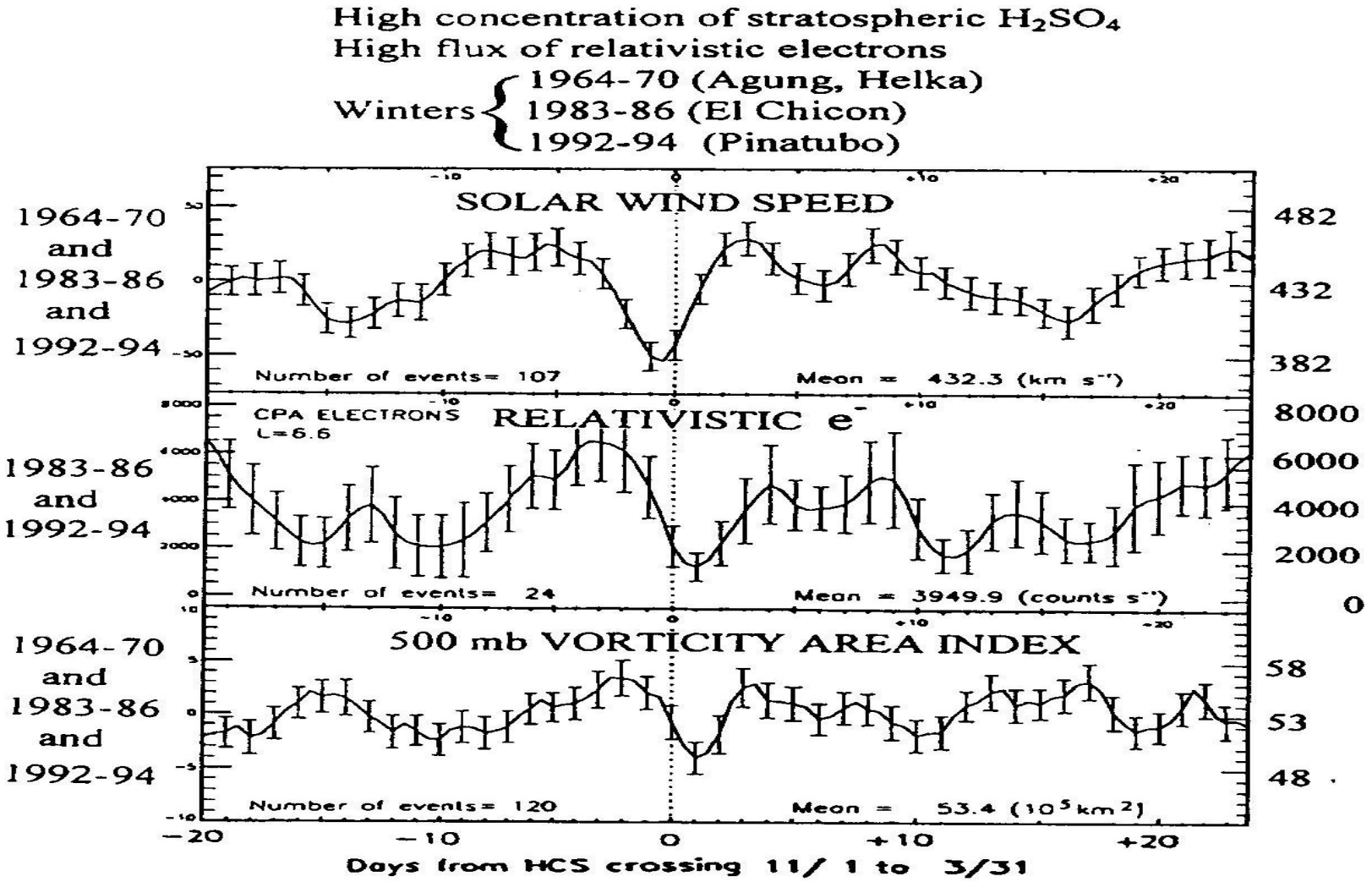

Superposed epochs, keyed to days of sector boundary crossings, November-March.
Top: Solar wind speed. Middle: MeV electrons from geosynchronous orbit.
Bottom: Northern hemisphere Vorticity Area Index.

Variability of outer radiation belt electrons

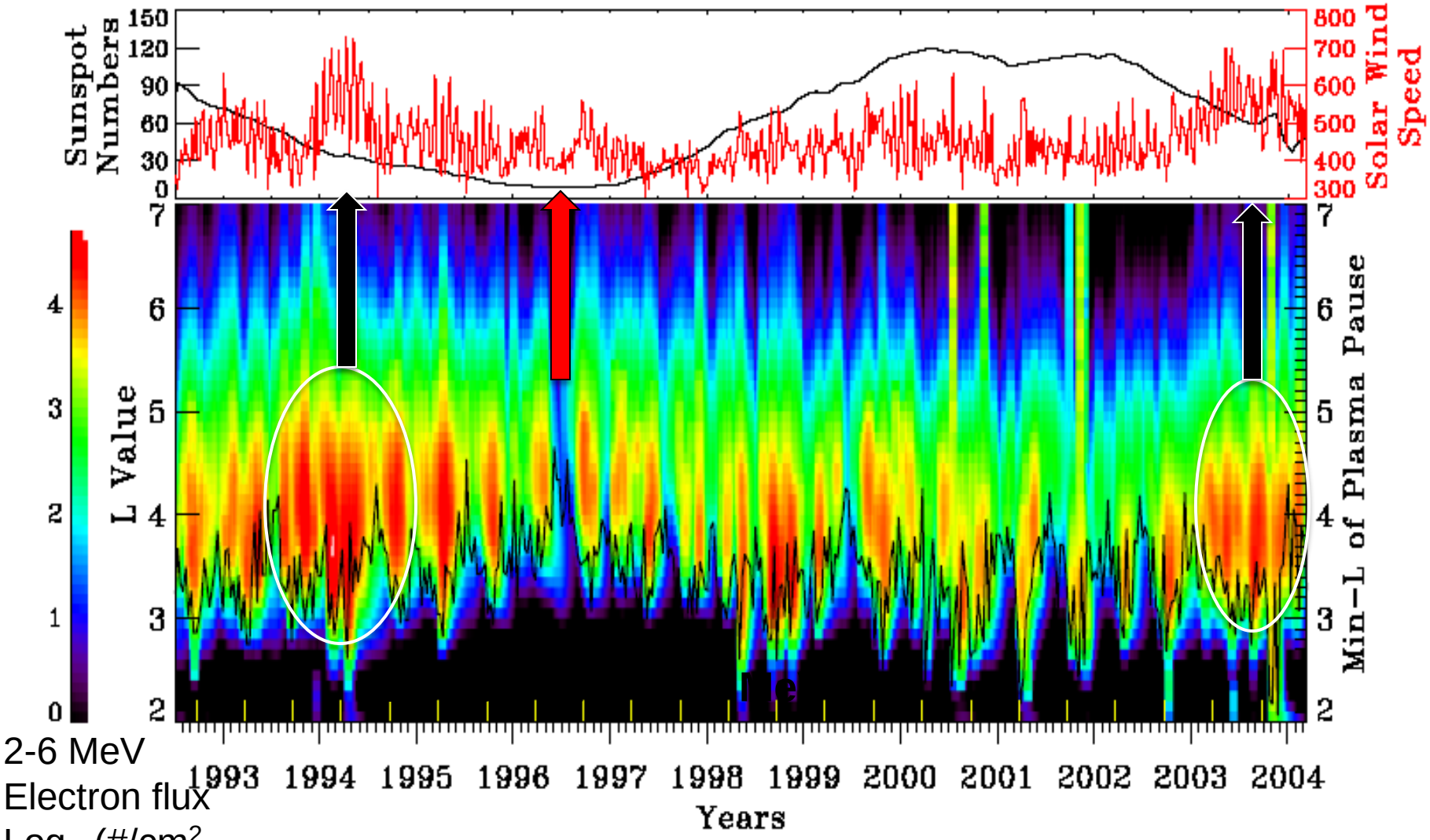

2-6 MeV Electron flux Log_{10}(#/cm^2-s-sr) from SAMPEX

[*Li et al.*, GRL, 2006]

Vorticity Area Index changes keyed to either HCS crossings or minima in relativistic electron flux, correlated with minima in J_z

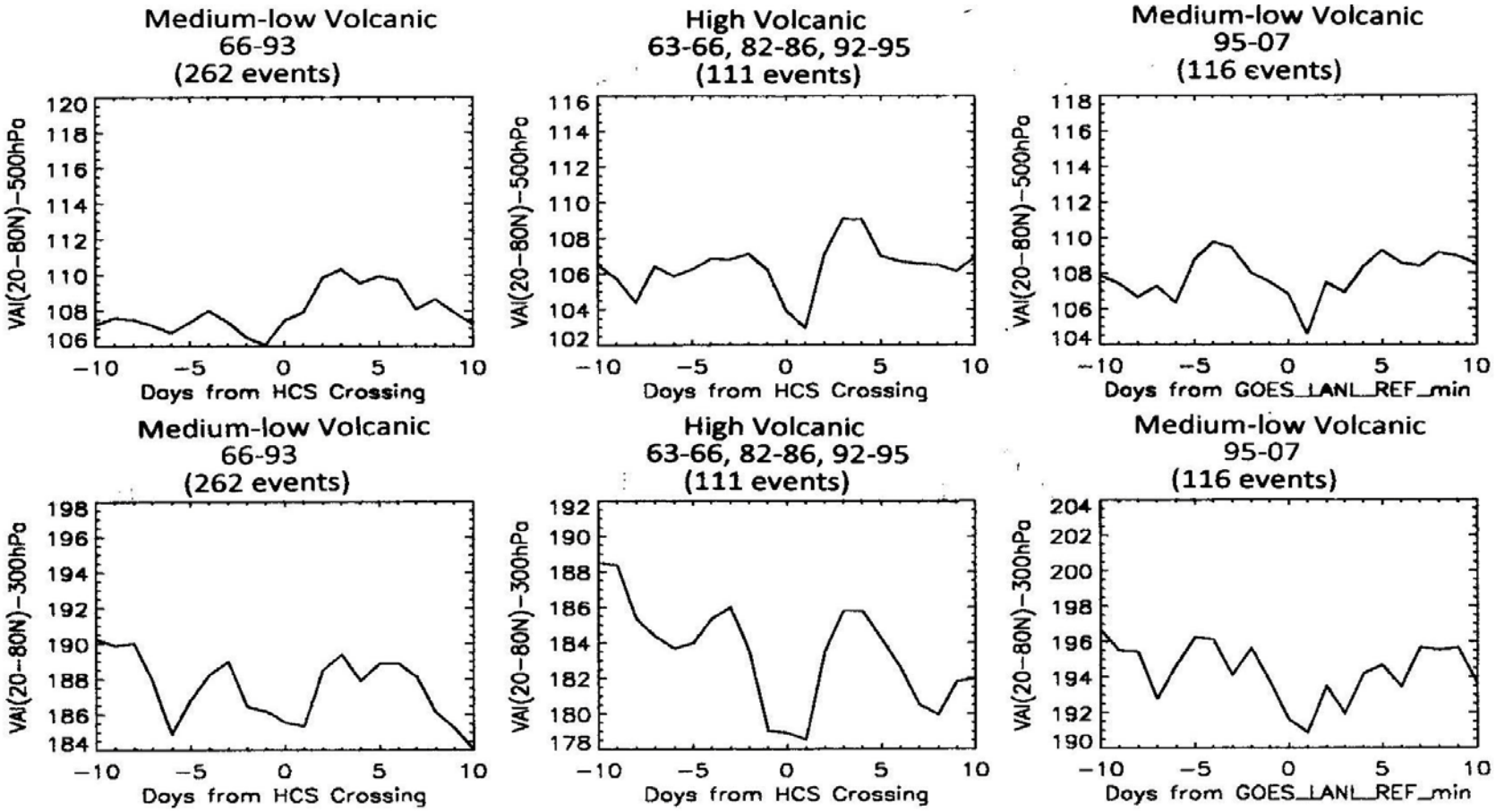

VAI response for medium-to-low stratospheric volcanic aerosol winters compared with high aerosol winters. Key days prior to 1995 are HCS crossings; from 1996 to 2007 are relativistic electron flux minima. From Tinsley et al. Adv. Space Res. 2012.

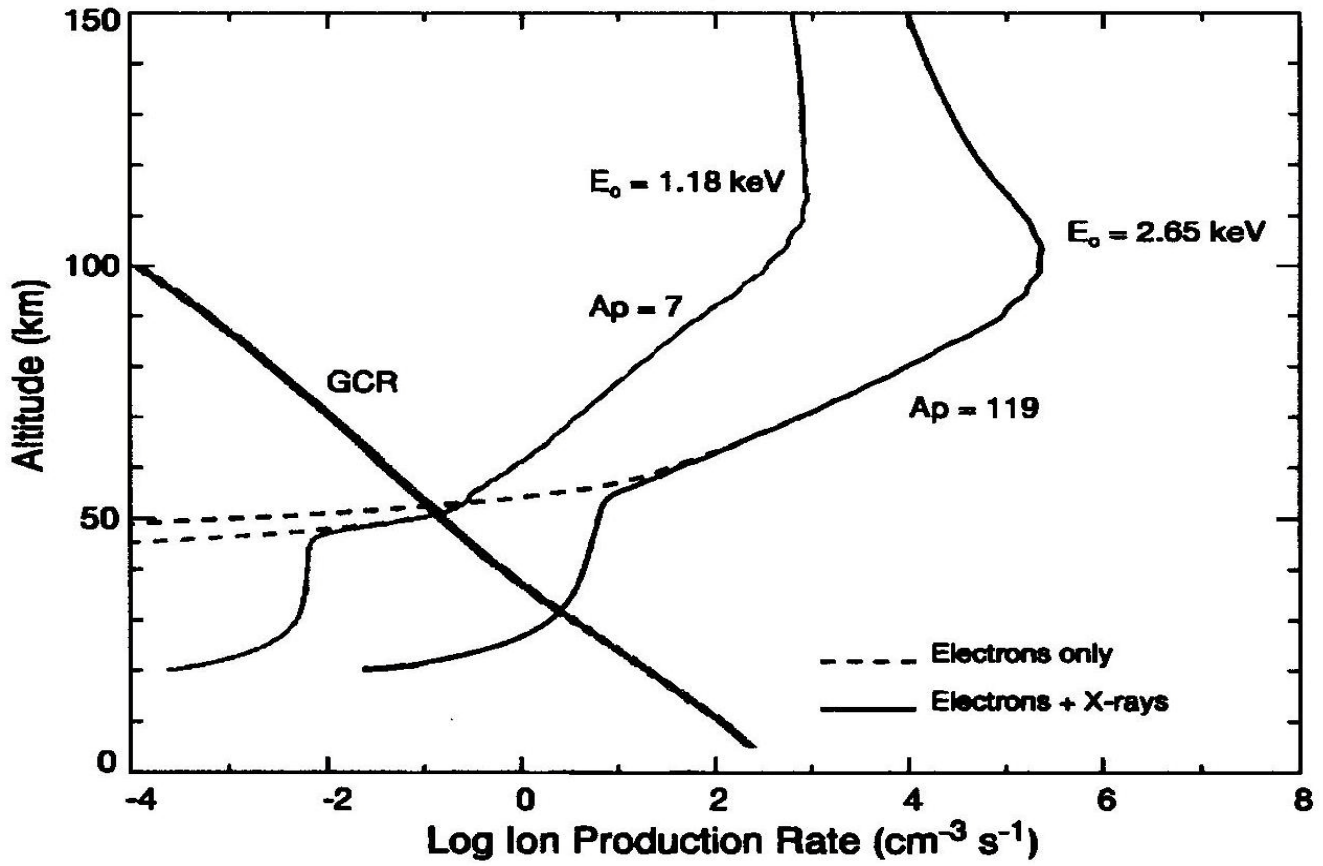

Ionization rate profiles for two events, both with fluxes of relatively low energy electrons in the auroral zone. Peak energy deposition was ear 100 km, with most Bremsstrahlung produced near 80 km, and penetrating to 20-30 km. However, at L-values of 2-3, the electron spectrum is characteristic of higher energies (SAMPEX) and precipitating 5 MeV electrons penetrate to 40 km altitude, and produce higher energy and more penetrating X-rays.

Effects of stratospheric and mesospheric volatiles and aerosol (speculative)

- Submicron nuclei from meteoric smoke and cometary dust
- At cold mesopause become coated with water, sulfuric acid, and nitrogen compounds, as in polar mesospheric clouds
- Sedimentation of aerosols
- Evaporation above warm stratopause, releasing H_2SO_4 and other vapors
- Ion mediated nucleation reduces mobility, as increasing numbers of polar molecules add to size and mass of ions; growth to large cluster ions.
- The growing cluster ions can reach a critical size (~ 1 nm radius) where they are stable as neutrals and continue to grow, to become nucleated aerosol particles, (to the extent that supplies of condensible molecules are available).
- The nucleated aerosol particles provide surfaces for ion attachment and recombination, thus reducing ion concentration.
- Additional condensation in cooler temperatures below stratopause (treated for 40 km altitude by Tinsley and Zhou, 2006).
- Aerosol surface area may be reduced by coagulation, but electric charge on aerosol particles may reduce coagulation

Effect on profile of conductivity of a layer of aerosols near 40 km

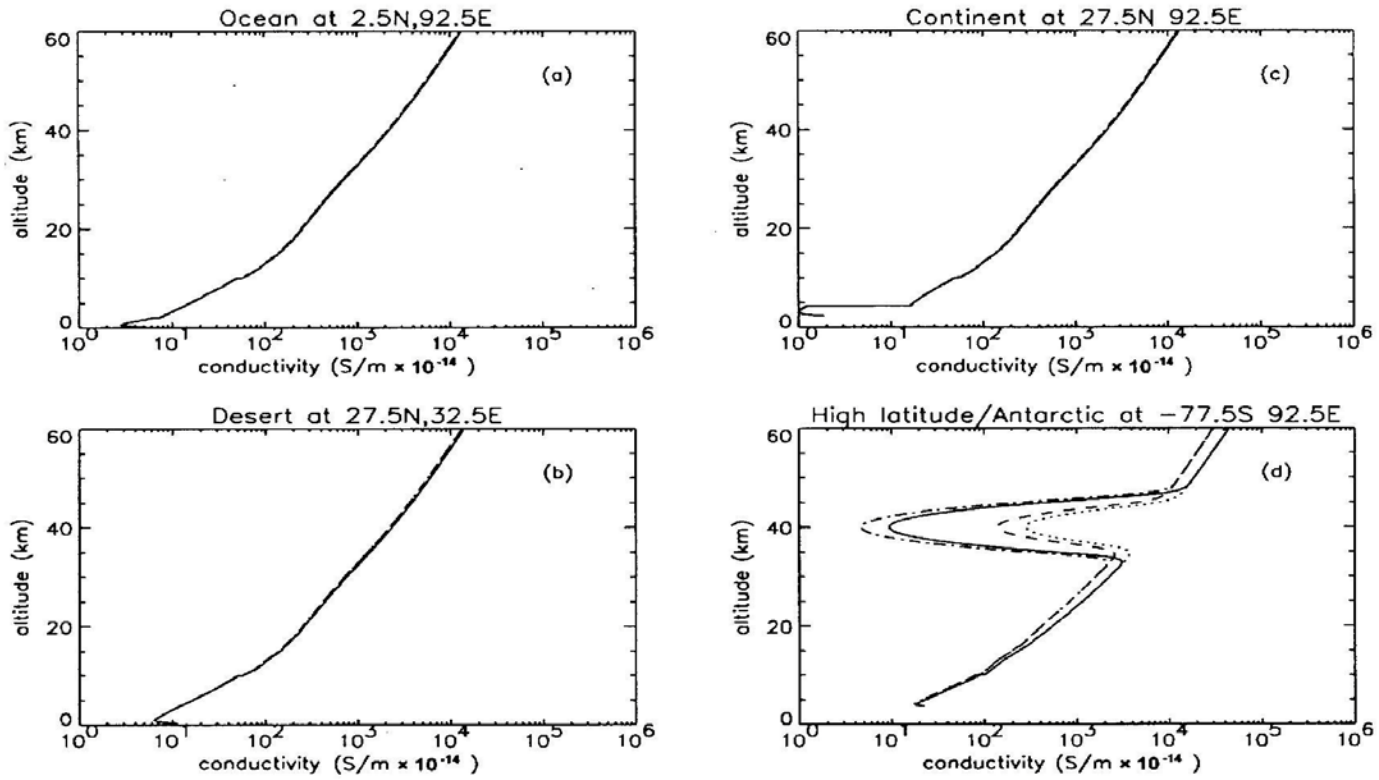

Effect on conductivity of the mixing ratio of H_2SO_4, measured at 20 km by solar occultation of aerosols, transferred to 40 km with 50% in the form of ultrafine aerosol particles of radius ~ 5 nm, on which ion attachment occurs. Tinsley and Zhou (2006). The solid and dot-dashed lines are for solar min and solar max respectively for the high levels of H_2SO_4 aerosols, and the dotted and dashed lines are for low levels.

SUPERPOSED EPOCH PLOTS WITH KEY DAYS MINIMA IN RELATIVISTIC ELECTRON FLUX AFFECTING VAI

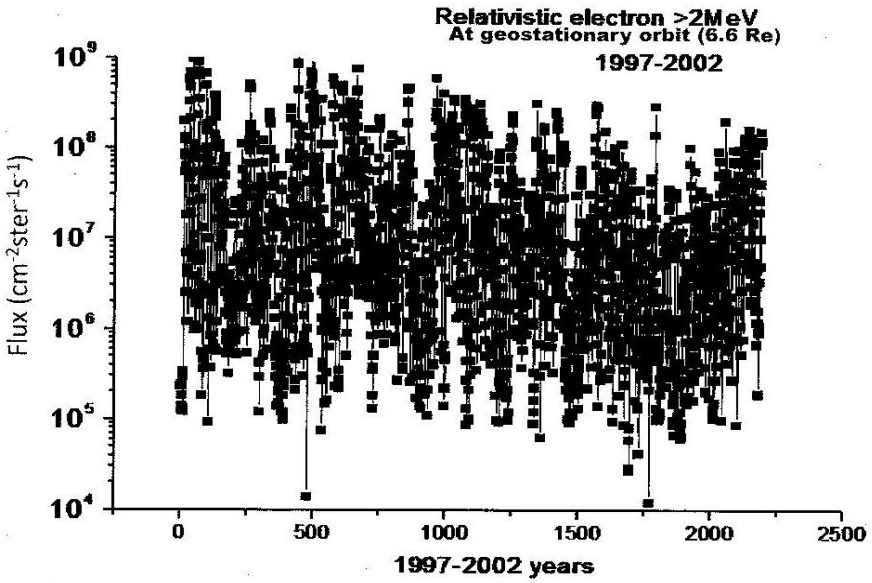

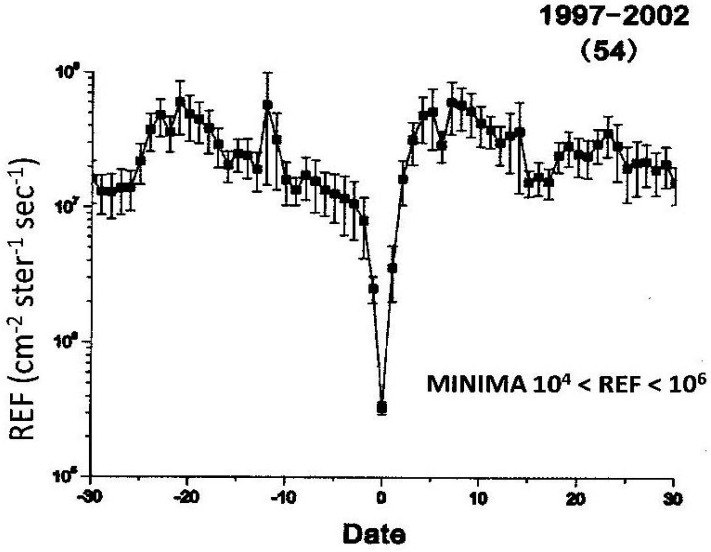

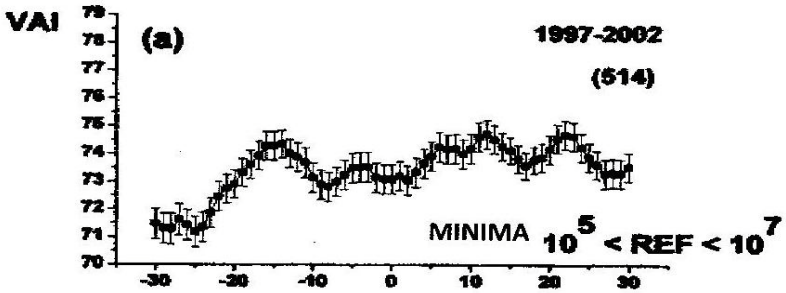

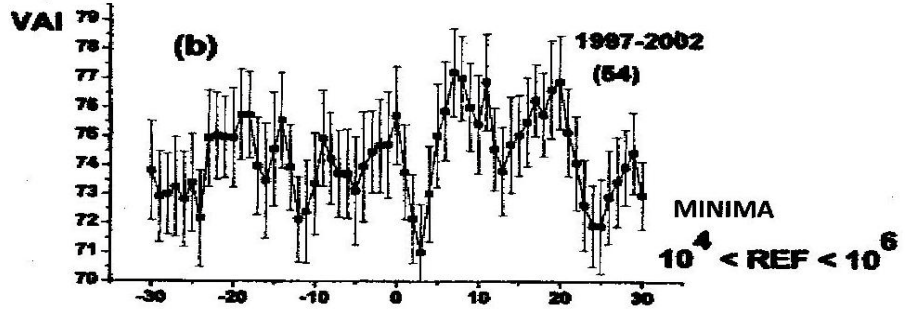

From Mironova et al., 2012

USE OF MINIMA IN SOLAR WIND SPEED

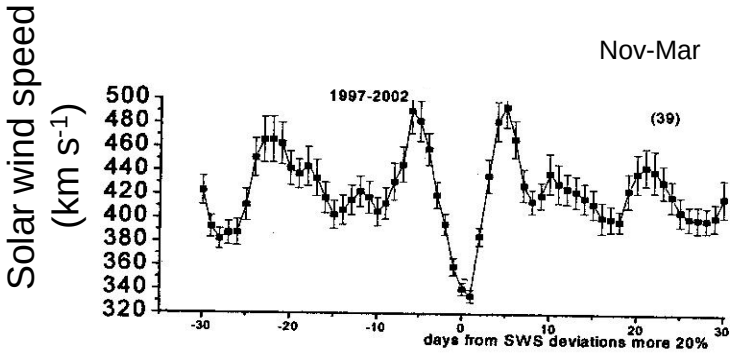

Solar wind, relativistic electrons and VAI, Mironova et al, 2011

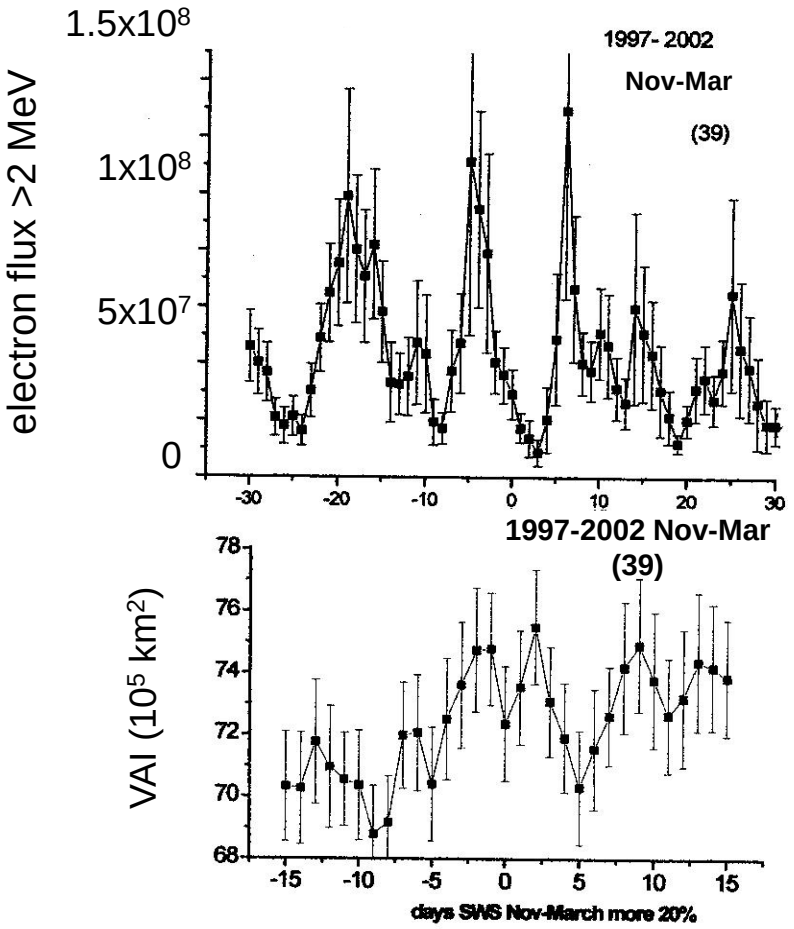

USING MINIMA IN REF, <10^6 cm^{-2} st^{-1} s^{-1}

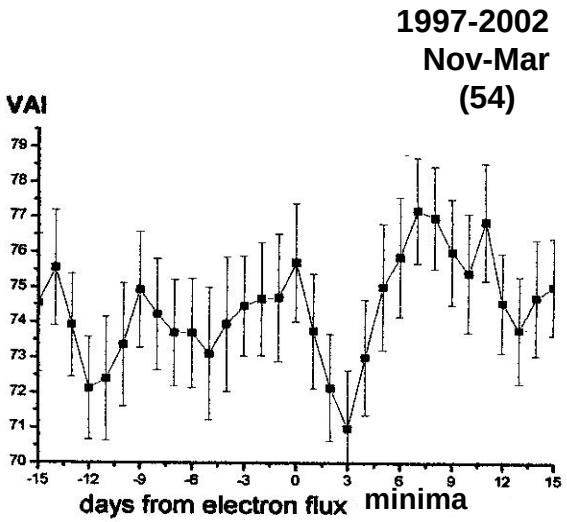

New results showing responses of the NAO and AO daily indices at solar wind speed minima, but only with high concentrations of volcanic H_2SO_4 aerosol in and above the stratosphere.

147 SWS minima, 1963-2011.

From Zhou et al. Advances in Space Research, in press.

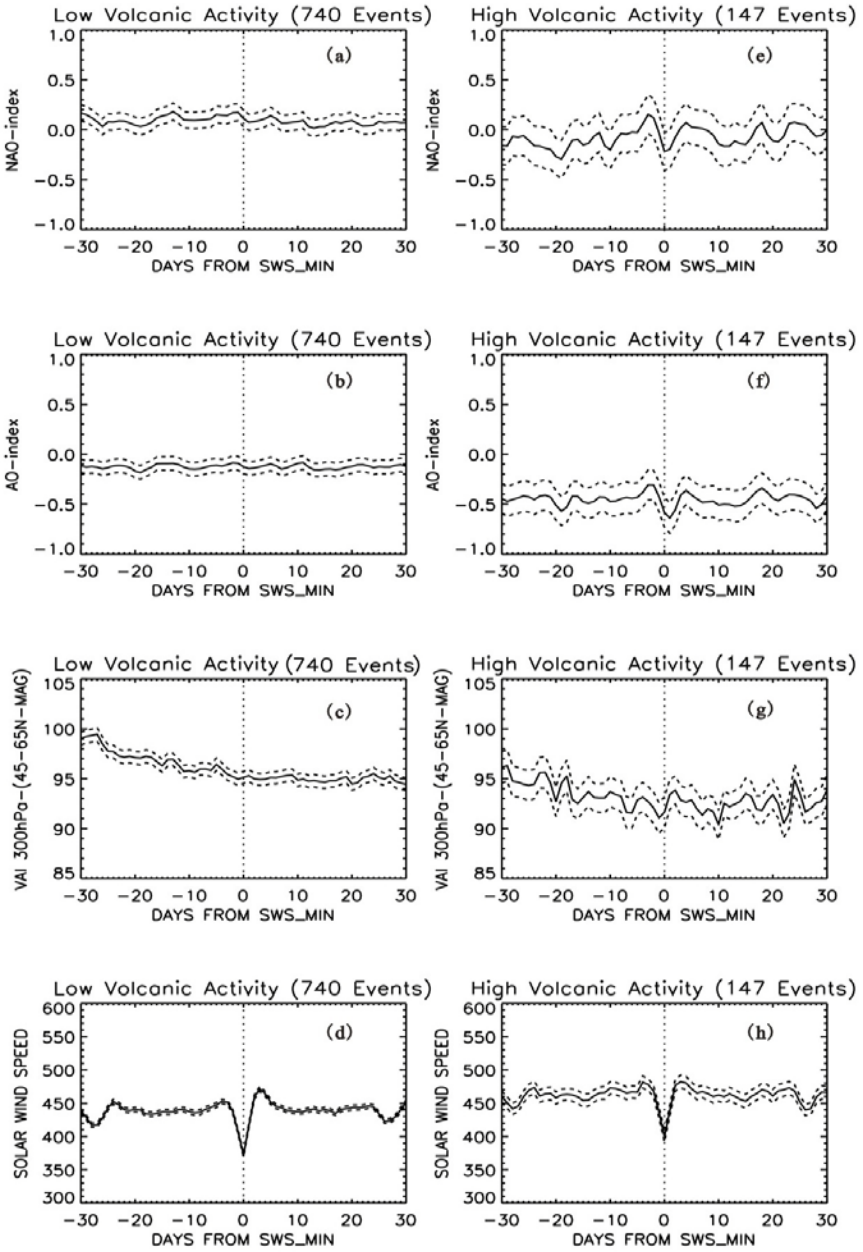

North Atlantic Oscillation Index

Arctic Oscillation Index

300 hPa Vorticity Area Index

Solar Wind Speed

Vorticity Increases with Solar Energetic Particles (a Jz proxy)

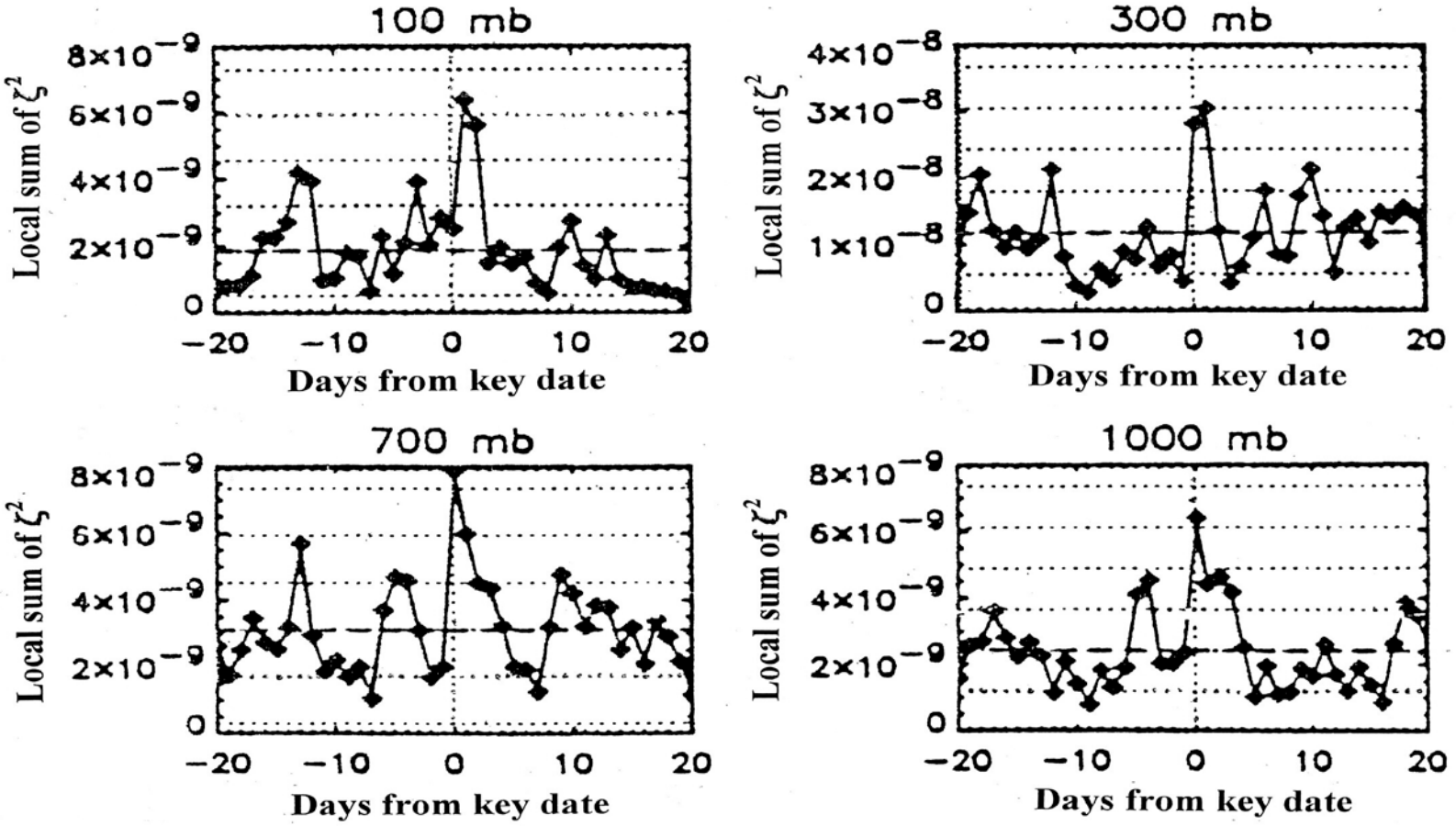

Variation of the squared vorticity (in s^{-2}) in North Atlantic region 50°-70° N, 0°-40°W, associated with the energetic SEP events. Dashed line is the mean level, and dotted lines are 1, 2, 3 etc. standard deviations from it.

From Veretenenko and Thejll, *J. Atmos. Solar Terr. Phys.*, *66*, 393, 2004

ION PAIR PRODUCTION RATES AT PEAKS OF SOLAR ENERGETIC PARTICLE EVETS

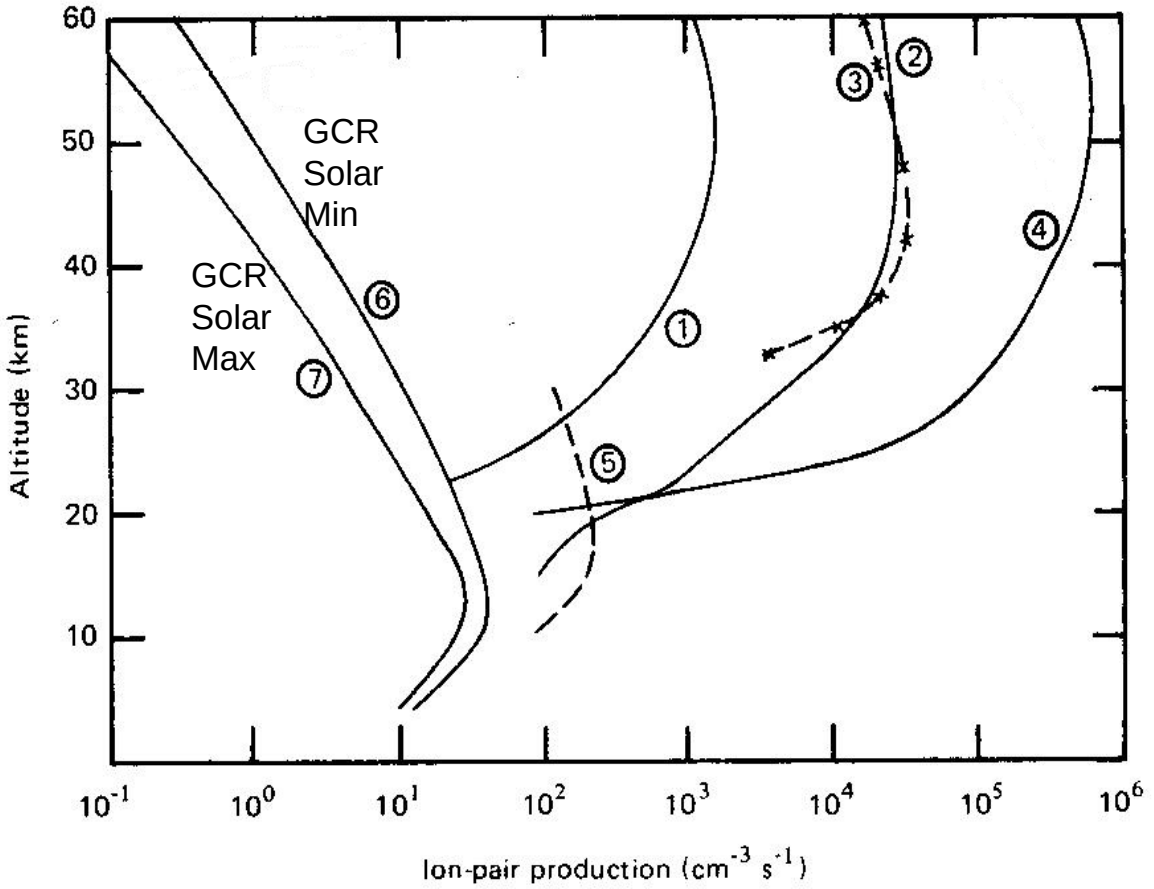

Figure 2.22. Ion-pair production rates due to solar protons (1, Nov. 2, 1969; 2, August 4, 1972, 1500–1600 UT; 3, August 4, 1972, 1508 UT; 4, August 4, 1972, 2200 UT; 5, September 29, 1961), galactic cosmic rays (6, ssmin; 7, ssmax); Curve 1, from Zmuda and Potemra (1972); 2, Kohl et al. (1973) and Bazilevskaya et al., (1973); 3, Reagan and Watt (1976); 4, Kohl et al. (1973); 5, Bryant et al. (1962); 6, 7, Webber (1962).

Data from Herman and Goldberg, “Sun, Weather, and Climate”, NASA SP-426, 1978. Injections of these particles produce ionization above 20 km considerably in excess of the galactic cosmic ray production. The ion-pair production rates are given per unit volume of air.

Diurnal Changes in Ionospheric Potential due to Thunderstorm Variations, and Effect on Polar Cloud Base Height

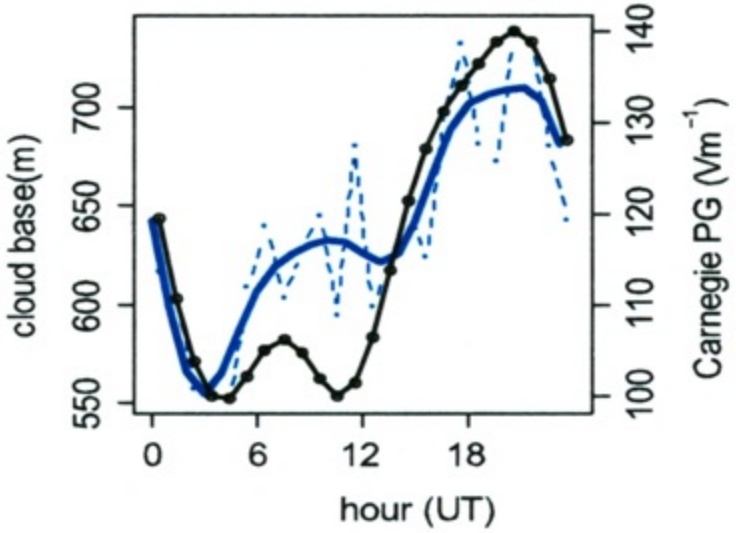

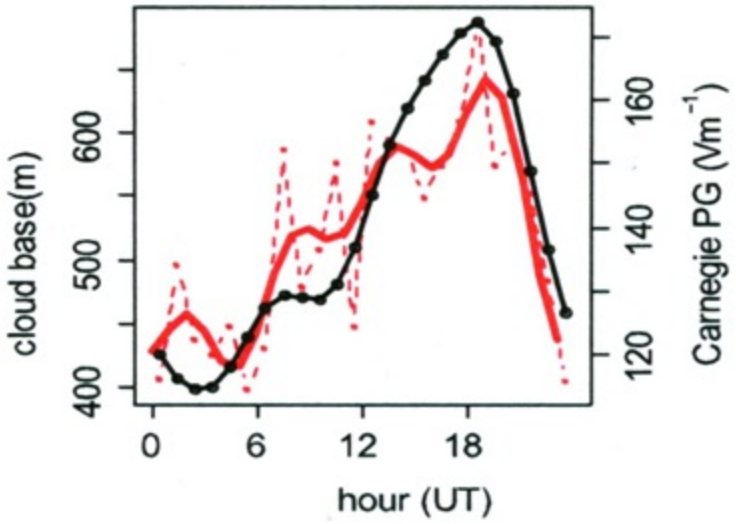

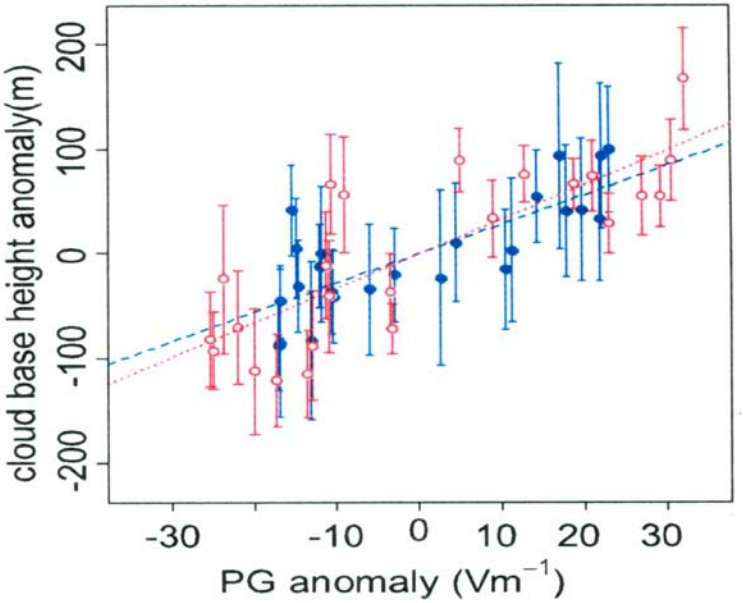

Changes in cloud base at Halley in Antarctic winter, (blue) and at Sodankyla in Arctic winter (red), correlate with changes in vertical potential gradient (black), and also with Jz. From Harrison and Ambaum (ERL, 2013)

Time variations in altitude and magnetic latitude of atmospheric electricity parameters for 92.5 E

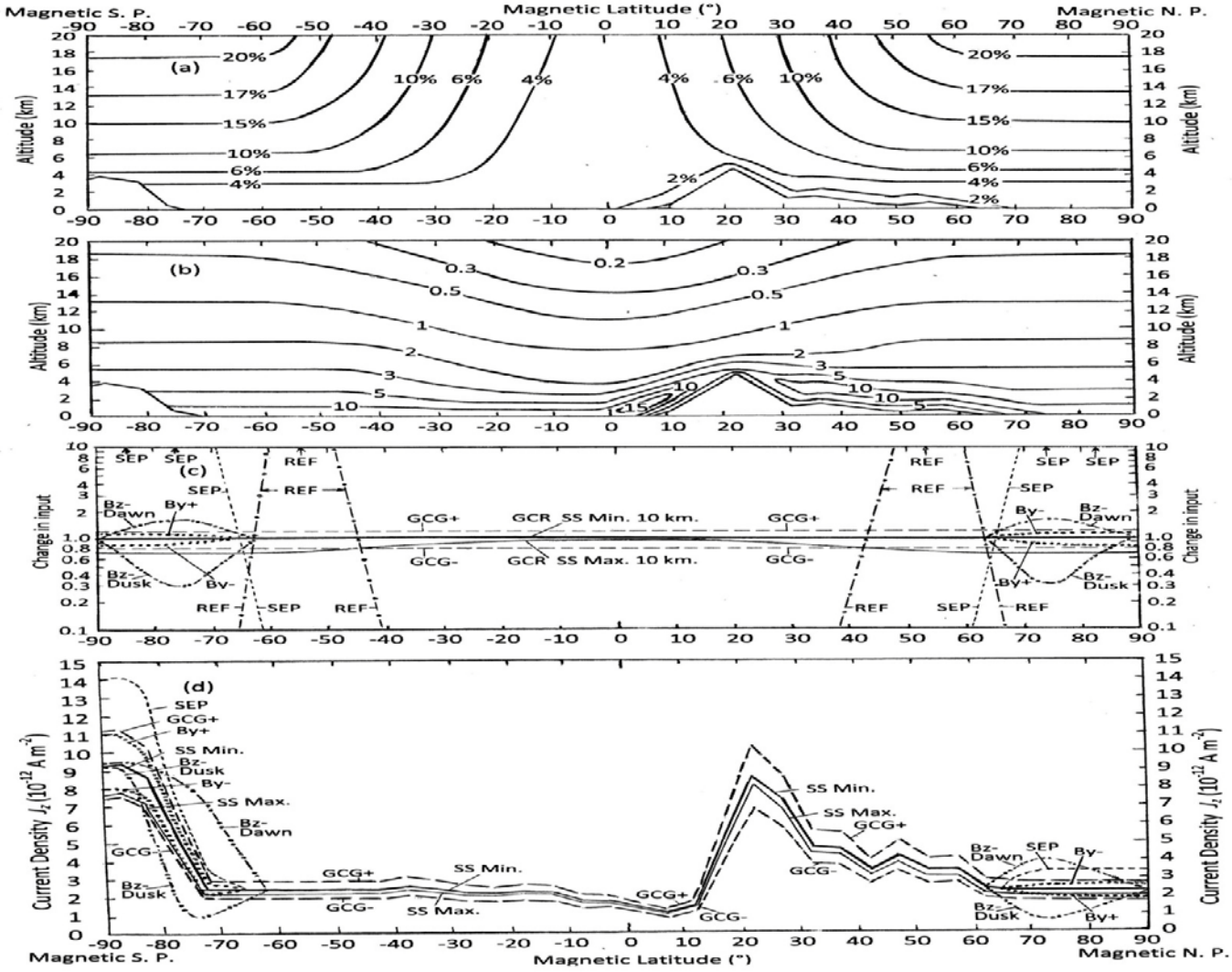

(a) % changes in ion concentration for 92.5 E from Tinsley and Zhou (2006)

(b) Resistivity changes (Ωm x10^{11}) (for 92.5 E)

(c) amplitudes of various inputs that modulate J_z

(d) Latitude distribution of J_z variations (for 92.5 E)

Inputs are galactic cosmic ray flux (GCR), relativistic electron flux (REF); solar energetic particles (SEP); solar wind (By+, By-, and Bz-); global circuit generator variations (GCG+ and GCG-). From Tinsley (2010).

Need for Quantification and Prediction of Space Weather Inputs

Solar wind magnetic sector structure (B_y, B_z, and V_x) are becoming quantifiable from interplanetary spacecraft measurements and predictable from observations of coronal holes and chromospheric structure, and could be used to predict V_i in polar cap regions

Solar energetic particles (mainly solar protons) are quantified by near-earth spacecraft, and could be statistically predictable from chromospheric magnetic structure.

Galactic cosmic ray fluxes modulated by solar wind magnetic fields are quantified by neutron monitor networks and spacecraft measurements. They could be predictable from spacecraft coronal mass ejection observations.

Relativistic electron fluxes are a strong function of solar wind speed V_x, and of ULF waves in the solar wind producing inward radial diffusion of trapped particles, and ion-cyclotron waves (Chorus) to energize them. There is a need for continuing low-Earth orbit measurements, and development of a predictive model of the flux and energy distributions as a function of geomagnetic latitude and solar wind parameters.

Plasmaspheric Hiss

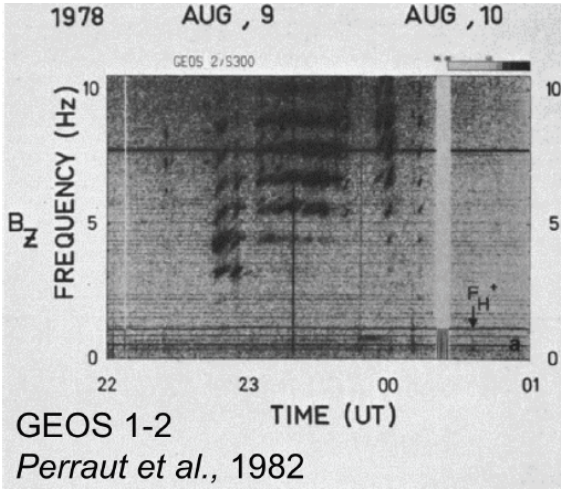

GEOS 1-2

Perraut et al., 1982

A variety of plasma waves in magnetosphere

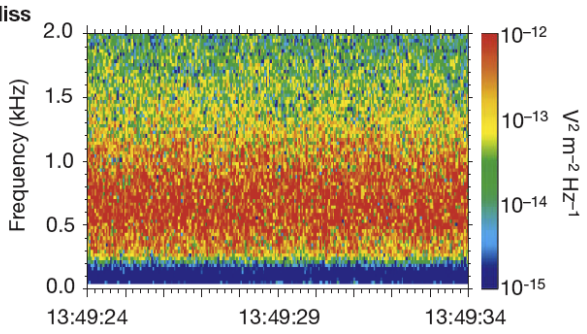

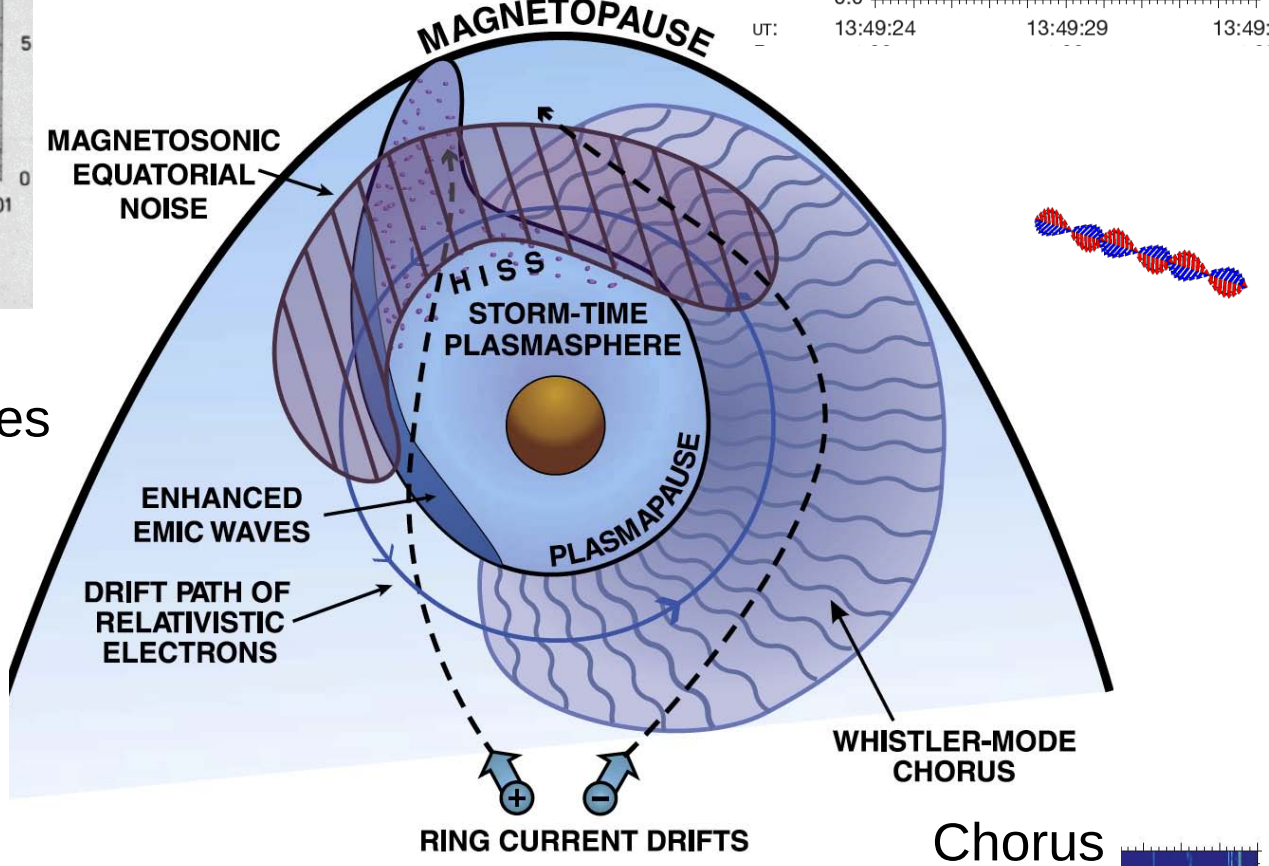

Electromagnetic Ion Cyclotron (EMIC) waves

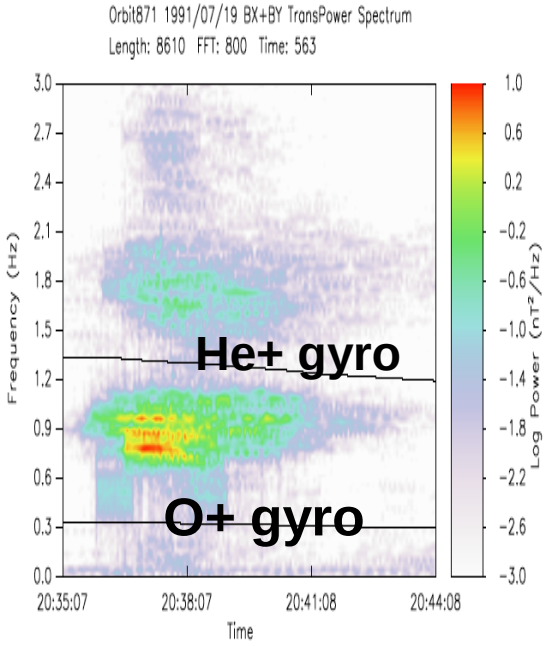

Chorus

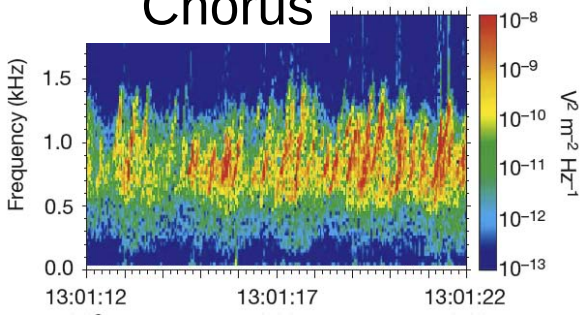

EFFECTS OF J_Z ON CLOUDS

Two effects involved:

(1) ACCUMULATION OF CHARGE

The flow of current density (J_z) through clouds and aerosol layers deposits electric charge on the droplets and the aerosol partiles

(Also, high charge generated by ice processes in deep convective clouds – responds to conductivity changes – not considered here)

(2) SCAVENGING OF NUCLEI

The electric charge on aerosol particles - importantly interstitial condensation nuclei CCN, and ice forming nuclei, IFN, - affects their rate of collision with droplets (in-cloud scavenging).

The charge can increase or decrease the scavenging rates, dependent on size, changing the concentrations and size distributions.

Size distribution changes in CCN produce size distribution changes in droplets, affecting coagulation, precipitation, latent heat transfer and cloud cover.

Scavenging of ice-forming nuclei by supercooled droplets promotes contact ice nucleation, releasing latent heat.

The latent heat changes cause storm invigoration, and in winter storms can cause changes in the amplitude of Rossby waves and blocking.

Schematic of Space Charge Accumulation, as in Oceanic Clouds

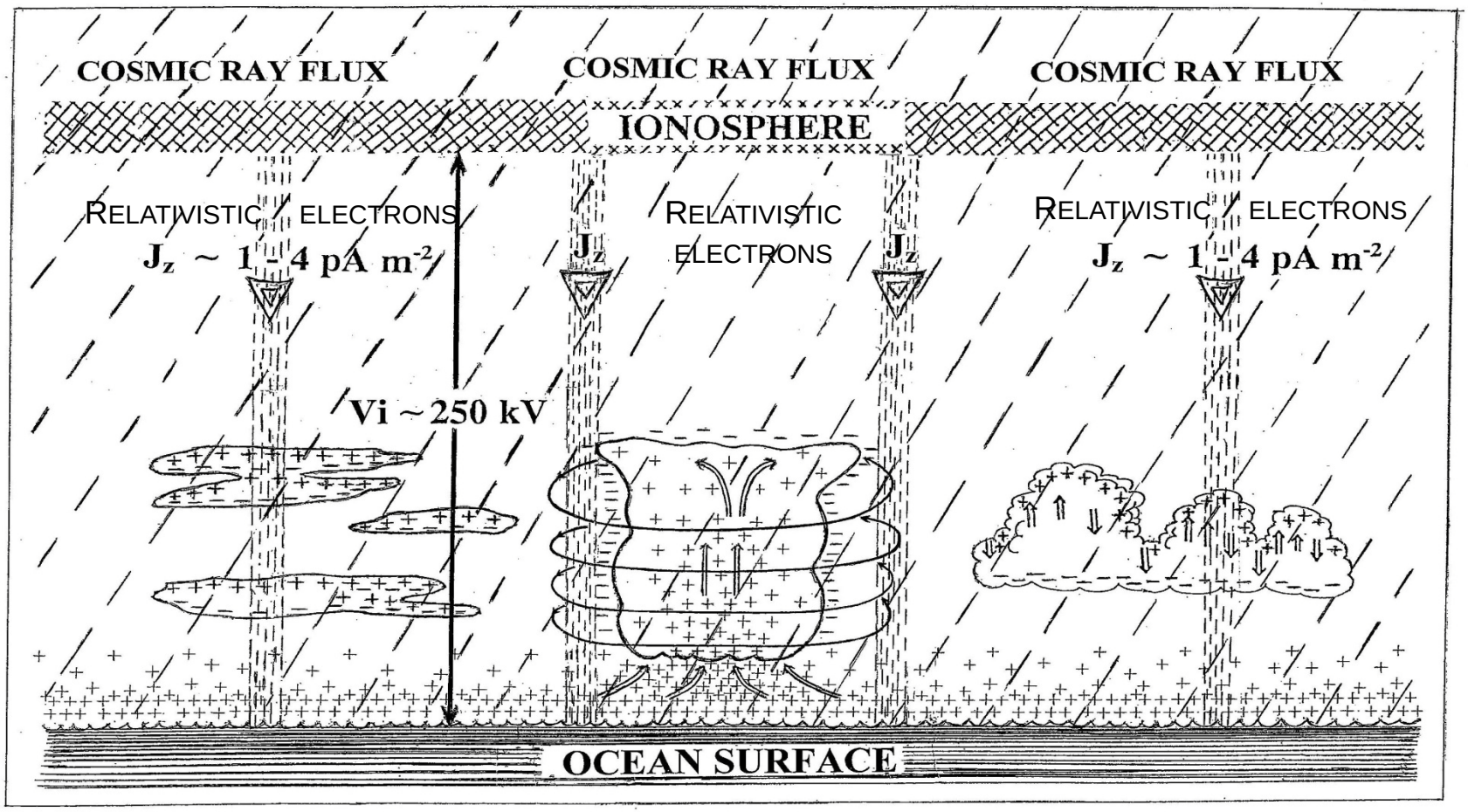

Variable cosmic ray and other space particle fluxes ionize the atmosphere.
In the magnetic polar caps the solar wind superimposes potentials on low latitude V_i.
The current density (J_z) depends on stratospheric and tropospheric column conductivity, and on V_i (Ohms Law).
Space charge is formed as J_z flows through conductivity gradients (Poisson's Equation).
Space charge attaches to aerosols in sea spray particles, haze, and fog near the ocean surface.
Space charge is convected into clouds by updrafts.

Accumulation of charge on ions, aerosol particles & droplets in layer clouds from J_z flow

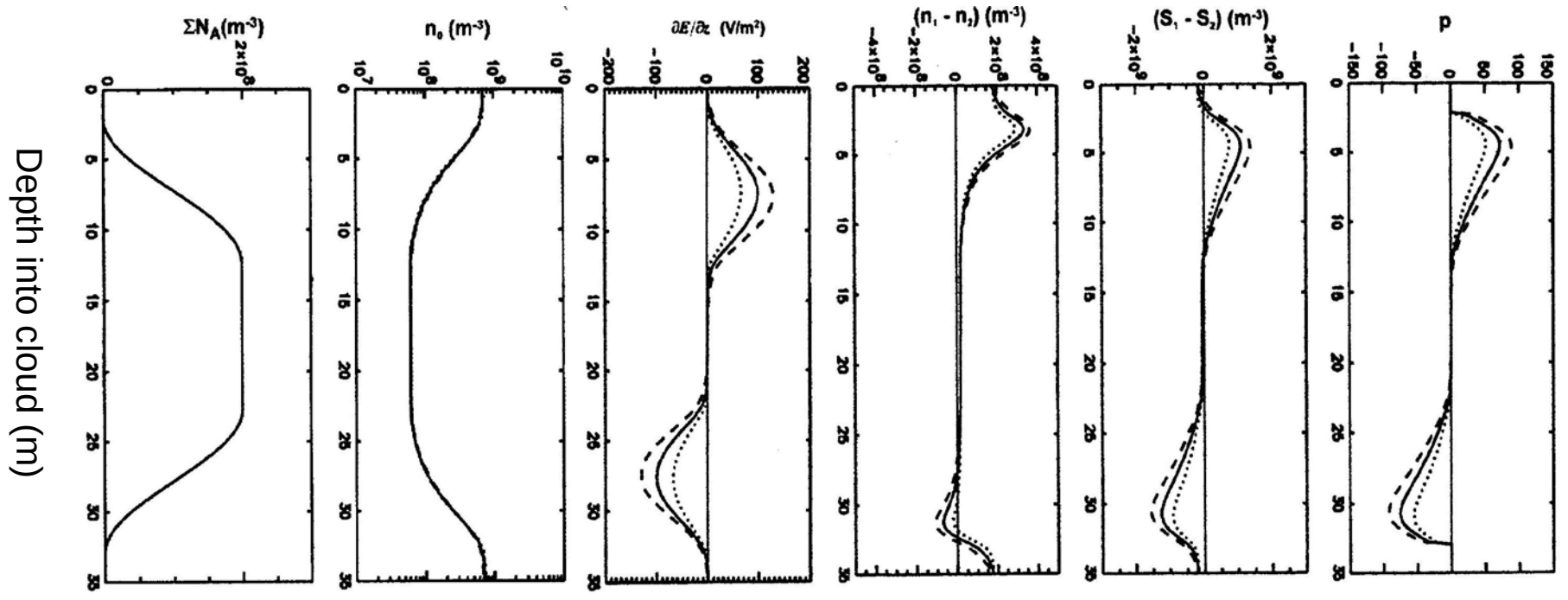

Droplet conc. Max. 2×10^8 m^{-3}

Ion conc. Max. 7×10^9 m^{-3} Min. 6×10^8 m^{-3}

Electric field gradient. Max. 130 V m^{-2}

Ionic space charge. Max. 3.5×10^8 e m^{-3}

Aerosol space charge. Max. 1.3×10^9 e m^{-3}

Droplet average charge. Max 80 e

Dashed line is for current density $J_z = 4 \times 10^{-12}$ A m^{-2} ; solid line 2×10^{-12} A m^{-2}; dotted line 1×10^{-12} A m^{-2}
Droplet radii 10μm, cloud boundaries 10 m thick, aerosol radii 0.04μm, altitude 4 km
The charging time constant is about 30 minutes. From Zhou and Tinsley, JGR, 2007.

Very much higher charges are observed in deep warm clouds and thunderclouds (Pruppacher and Klett, 1997). It is not known how much is inductive (proportional to J_z) as in Grenet-Vonnegut electrification, and how much is non-inductive (independent of J_z).

AIRCRAFT MEASUREMENT OF DROPLET CHARGES, Ochs and Beard, 2012

Counter flow virtual impactor mounted on a NCAR C130 wing

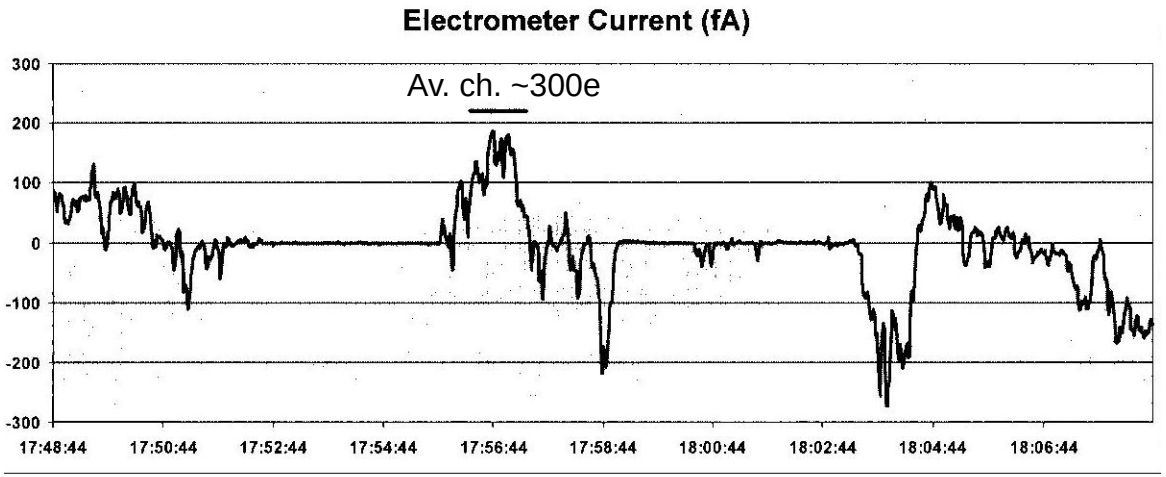

Sample of measured average droplet charges when the aircraft was in the layer cloud (e = elementary charge of 1.6 x 10^{-19} C).

- The observations showed regions with both positively and negatively charged average droplet charges, with average charges ranging from +300e to -300e.
- Many other aircraft and balloon measurements show that almost all layer clouds contain droplets with comparable average charges.
- Diffusion charging theory implies charges on aerosols and droplets proportional to their radii.
- In thunderstorms and deep convective clouds the charges are orders of magnitude greater.

Needs for modeling of charging of layer clouds, convective clouds and cyclone clouds

For layer clouds, one-dimensional models of cloud boundary charging have been given by Zhou and Tinsley (2007, 2013). There is a need to extend these to 3-dimensions for application to convection in the cellular structure of marine stratocumulus.

For convective clouds, charged aerosols from near the surface, with charge originating with Jz, are carried by updrafts into the body of the cloud.

In barotropic convective clouds (summertime cumulus), a simple model has been given by Vonnegut et al., (1962).

For baroclinic oceanic cyclones, an outline has been given by Tinsley (2012). There is a need for detailed 3-dimensional models in both barotropic and baroclinic systems.

These provide the inputs for use of parameterized scavenging rates in realistic models of cloud formation and development

In oceanic cyclones space charge is carried into the cloud in updrafts in the hook or comma cloud, which becomes the location for maximum space charge and invigoration.

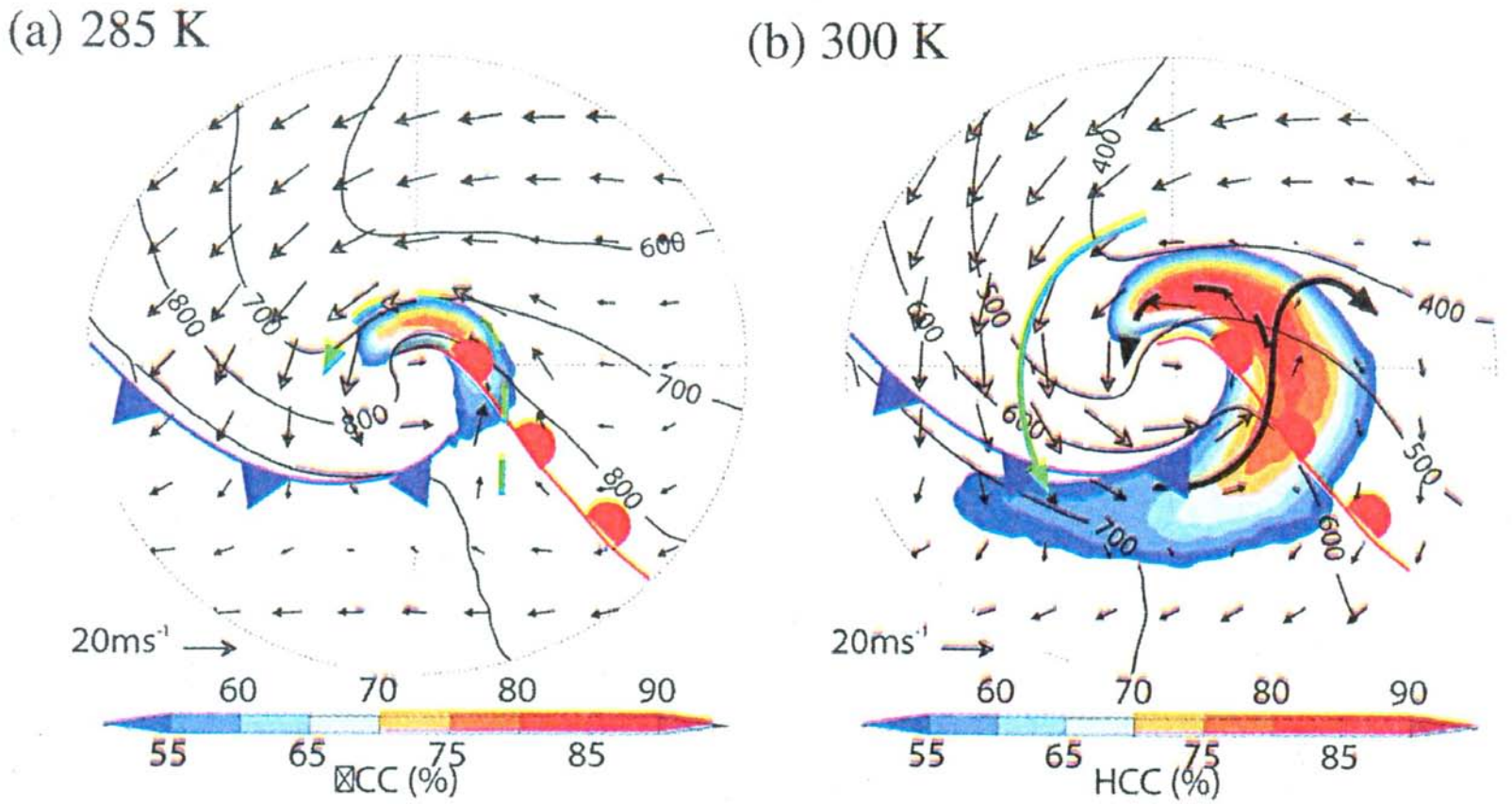

The panels are (a) 285K and (b) 300K potential temperature isentropic surfaces. Pressure is shown as solid contours, winds as arrows. The percentage cloud cover is in solid colors. COMPOSITE OF 200 MOST INTENSE NORTHERN HEMISPHERE EXTRATROPICAL CYCLONES IN THE LAST 20 YEARS (BAMS, 2012)

Electrical effects on scavenging rates: simulations and parameterizations

Following the work of Pruppacher and his students in the 1970s, TRAJECTORY SIMULATIONS for in-cloud particle scavenging have been made, without considering diffusion, by Tinsley et al. (2000, 2001), Tripathi and Harrison (2002), Tinsley et al. (2006), Tripathi et al. (2006), and Zhou et al. (2009).

SIMULATIONS considering diffusion, which dominates for smaller particles interacting with smaller droplets, have been made by Tinsley (2012).

PARAMETERIZATIONS of simulations without diffusion have been given by Tripathi et al. (2006). PARAMETERIZATIONS of simulations with diffusion are due to Tinsley and Leddon (2013) and by Tinsley and Zhou (in preparation).

Together with realistic models of cloud charging, these parameterizations provide the inputs for use to model scavenging rates in realistic models of cloud formation and development.

Simulations of particle scavenging without diffusion

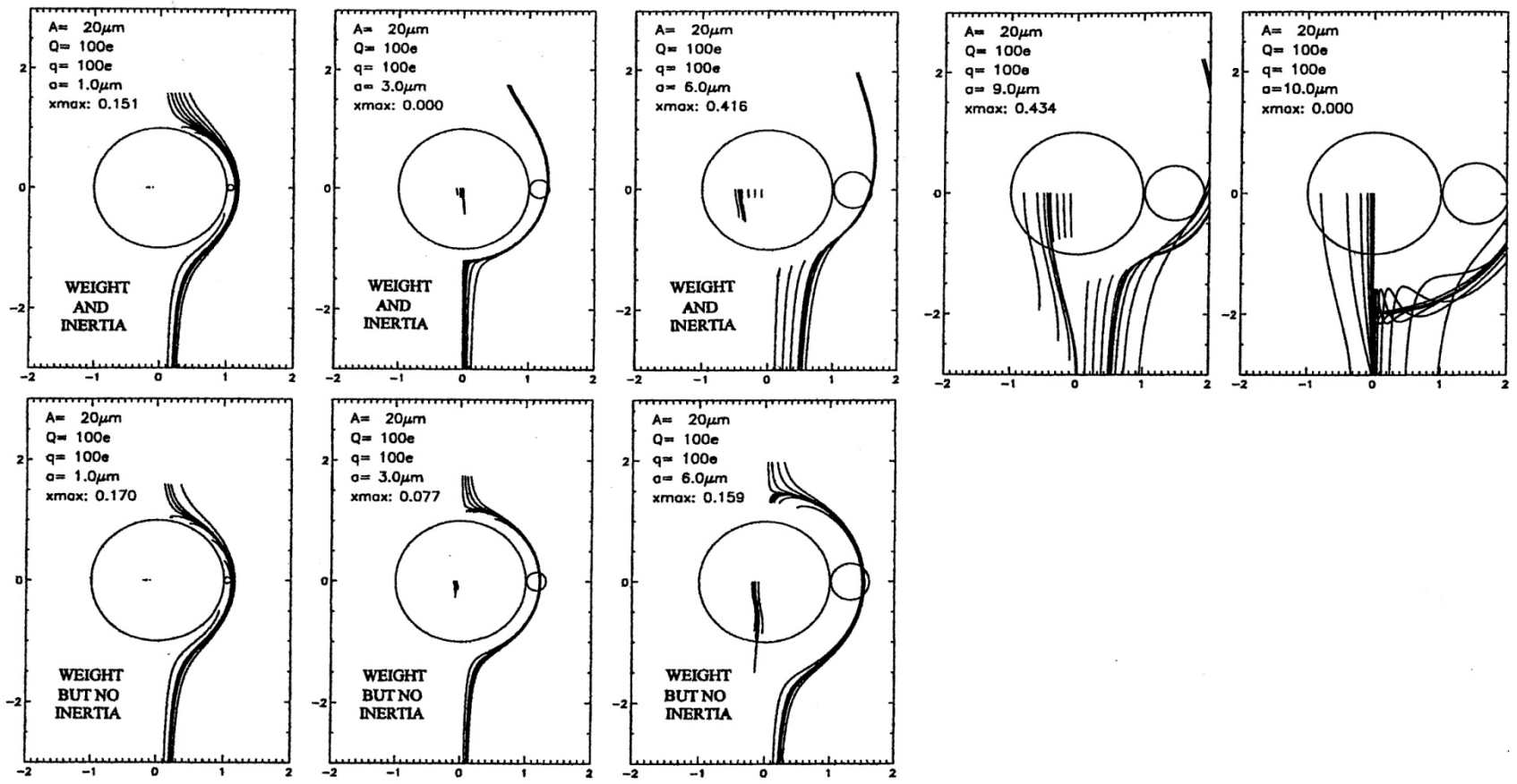

Droplet radius 20 μm. Particle size increases from 1 μm to 20 μm from left to right. Inertia prevents rear capture - compare top and bottom panels. For 3 μm and 10 μm particles their weight counteracts flow in the stagnation region.

Simulations of particle scavenging with diffusion

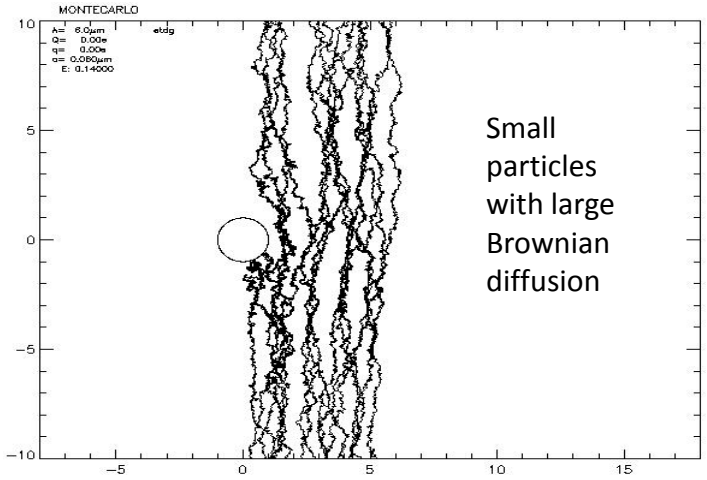

Typical small uncharged aerosol lifetime against Brownian scavenging ~ 20 minutes. Attraction by opposite sign droplet and particle charges reduces this lifetime.

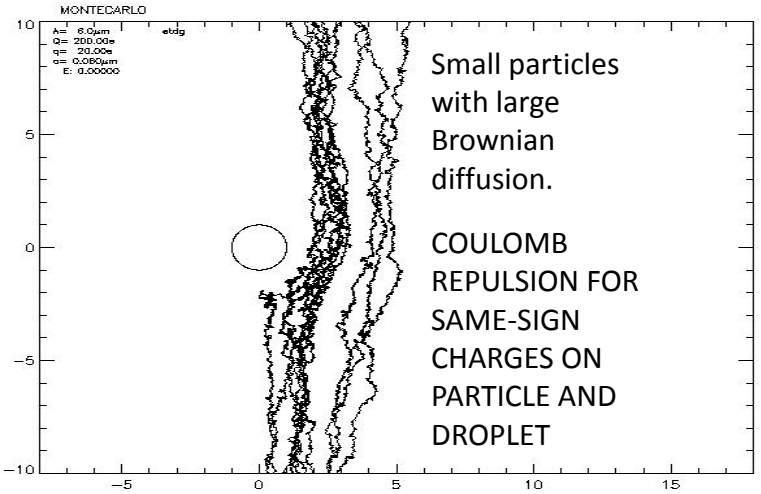

Long range repulsion (same sign charges) decreases scavenging rate, increases lifetime against scavenging.

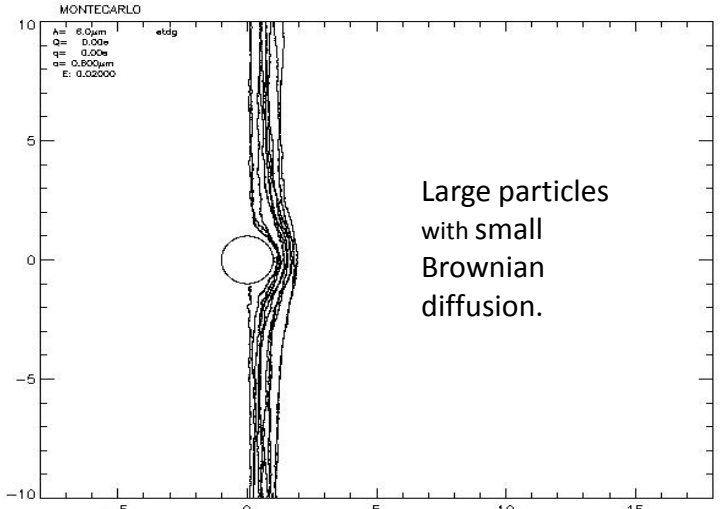

Low scavenging rate for typical large uncharged aerosol or evaporation residue; Stokes flow carries particle past droplet.

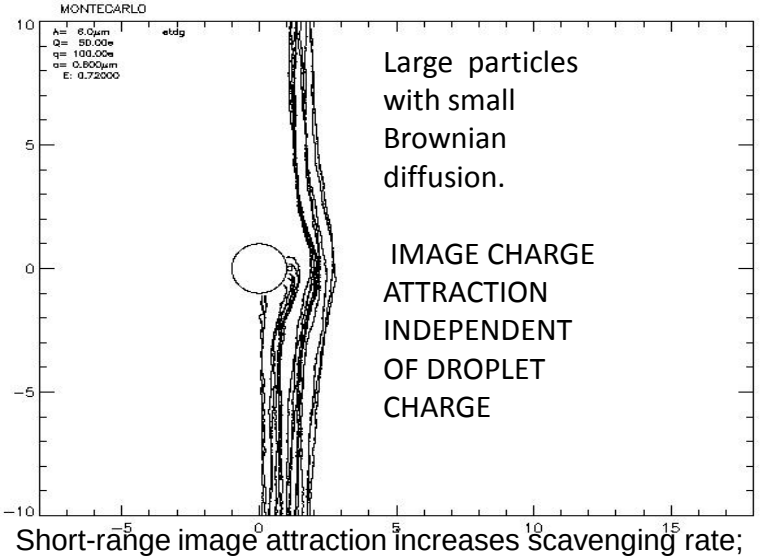

Short-range image attraction increases scavenging rate; reduces concentrations of large aerosol particles or charged evaporation residues.

Fig. 1

Scavenging rate coefficients for charged aerosol particles and droplets

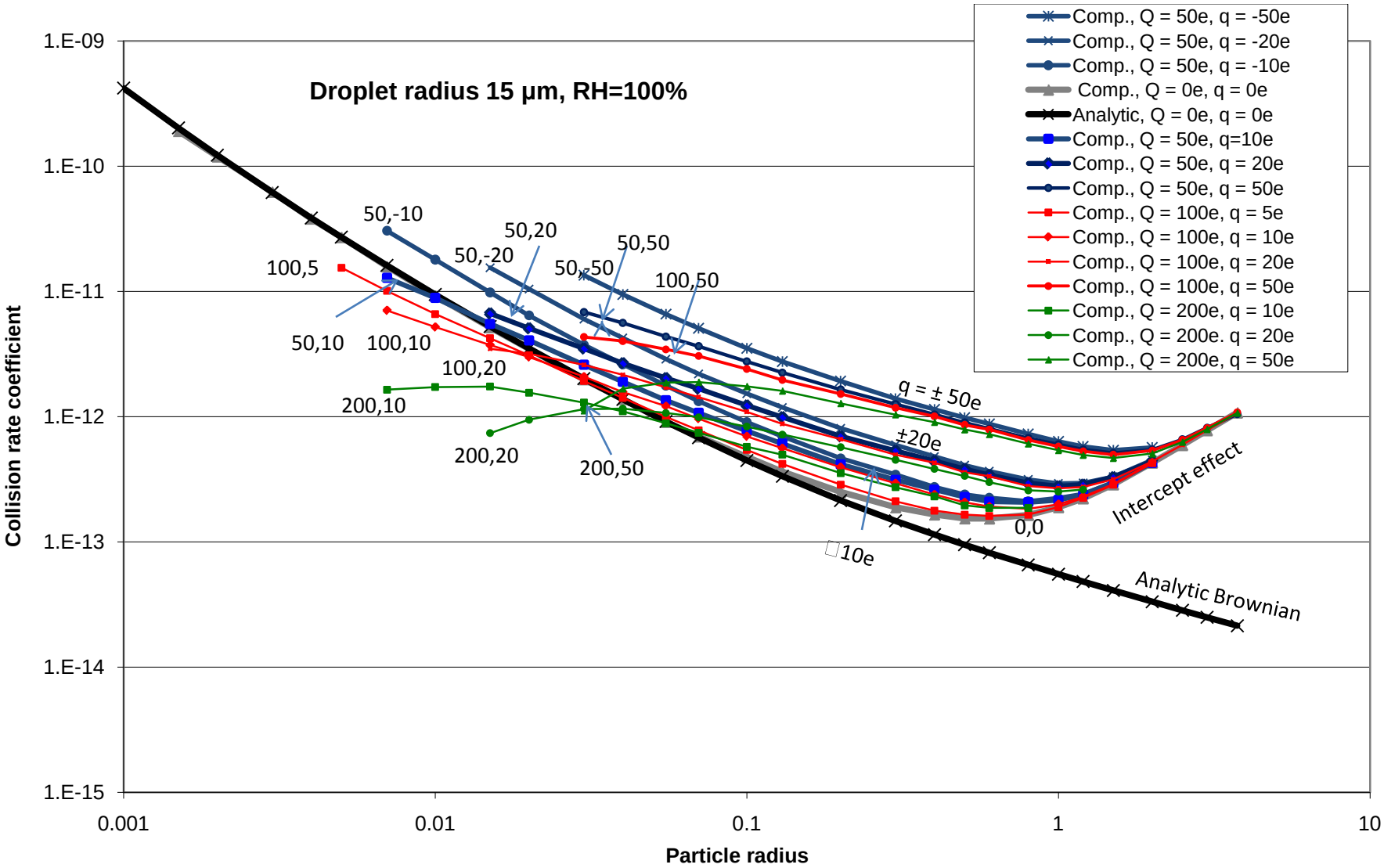

Collision rate coefficient ($m^{-6}s^{-1}$) for aerosol particles, of radius 0.005 μm to 3.75 μm, with droplets of 15 μm radius. Curves are labeled by droplet and particle charges 'Q,q'. The asymptotic change in electro-scavenging rate for larger particles is approximately proportional to the square of charge on the particle.

Quadratic variation of rate coefficients with charge, for q/Q same sign, for altitudes 1013 hPa to 50 hPa

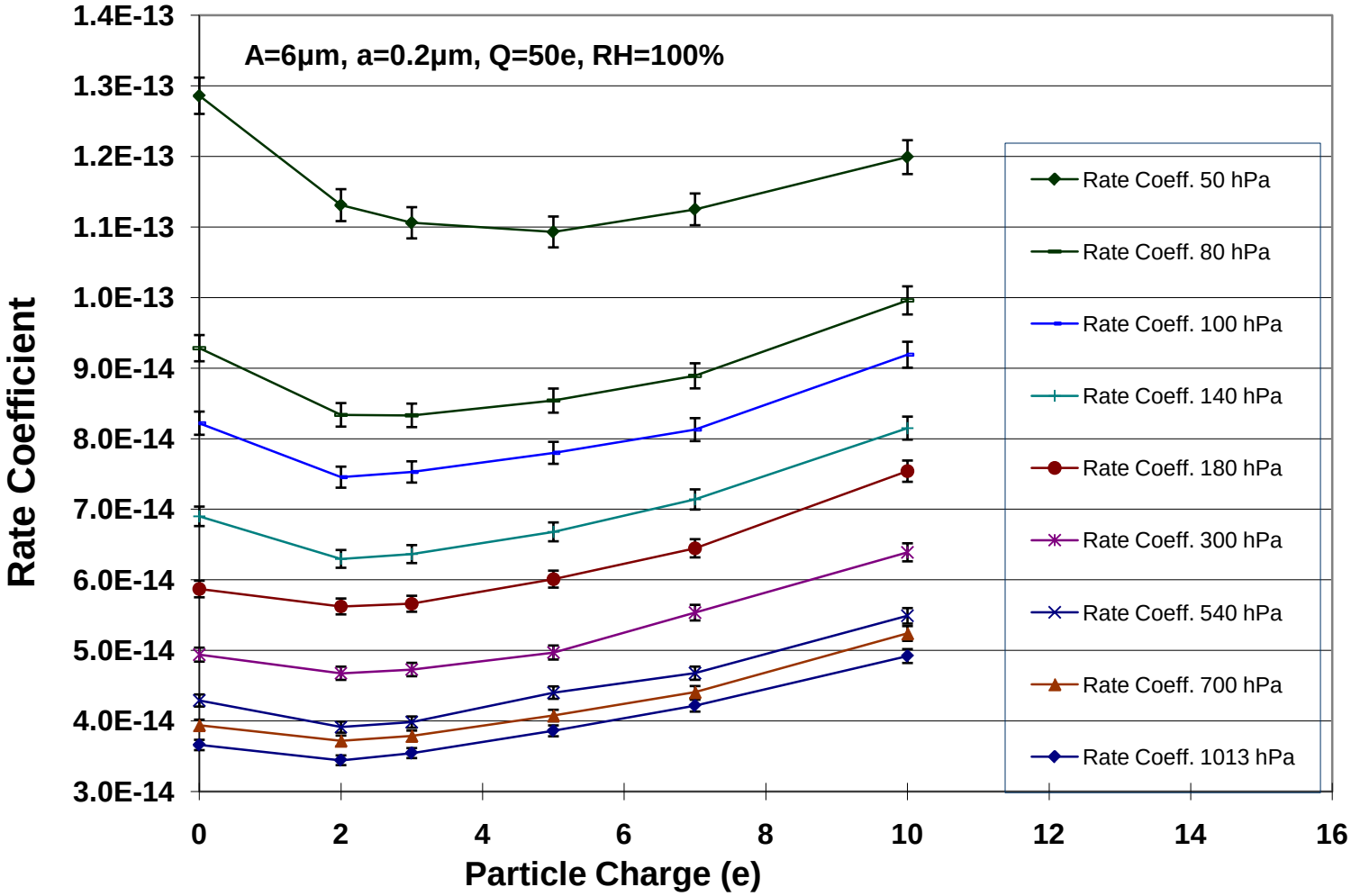

The rate coefficients first decrease with increasing particle charge q, (effect of electro-anti-scavenging for same-sign Q, proportional to Qq) before they increase (effect of electro-scavenging proportional to q^2.

Pathways from microphysical to cloud-scale changes

- From electrical changes in scavenging of particles (notably cloud condensation nuclei, CCN, and ice-forming nuclei, IFN) to changes in cloud dynamics and cloud cover:

- Pathway 1. CONTACT ICE NUCLEATION. IFN are generally larger than 0.5 μm radius, and the electrical effect is to increase the collision rate independent of the sign of Q/q. For droplets carried by updrafts above the freezing level, freezing does not occur until cooled below -15°C, unless contact ice nucleation occurs when the -5°C level is reached. Thus electro-scavenging in clouds with radiative cooling or weak updrafts have greater initial ice production, releasing latent heat of freezing, increasing updraft speed. For layer clouds there may be cloud cover changes.

- Pathway 2. CCN CONCENTRATIONS AND SIZE DISTRIBUTIONS . CCN radii are from 0.03 μm to several μm. The electrical effects on CCN can be increases in scavenging rate for larger particles, 'electro-scavenging', decreasing their concentration independent of the sign of Q/q. 'Electro-scavenging' also applies to CCN of all sizes with negative Q/q. Q/q is predominantly positive in space charge, with 'electro-anti-scavenging' for smaller CCN, with concentrations remaining higher than for zero charging. The lifetime of CCN in an air mass is one to ten days. In later cycles of evaporation/condensation the CCN changes result in decreases of the concentration of large droplets and increase in those of small droplets. This reduces the rate of coagulation and initial precipitation, and updrafts carry more droplets above the freezing level. This produces more ice and increases the vigor and therefore the vorticity of baroclinic storms. It may also increase the amount of water released into the upper troposphere and change cloud cover.

Pathways from microphysics to cloud-scale changes - continued

- Pathway 3. EVAPORATION NUCLEI AS CCN. A special case of the previous pathways. The droplets, with their large size, carry much more charge than nuclei, and when droplets evaporate, the 'evaporation nuclei' retain that charge for 10 minutes or so. These highly charged nuclei have reaction rates one or two orders of magnitude more than the nuclei with equilibrium charge. Evaporation of charged droplets in downdrafts and in drier air entrained by turbulence near cloud boundaries often occurs in storms, and the highly charged evaporation nuclei are then rapidly scavenged. Again, the change in CCN concentration can subsequently affect storm development.
- Pathway 4. EVAPORATION NUCLEI AS IFN. Turbulence and entrainment at cloud tops, if above the freezing level, can result in highly charged evaporation nuclei that can act as IFN in contact ice nucleation, promoting freezing and changing storm dynamics and cloud cover.

- Pathway 5. IN-CLOUD SCAVENGING OF IMMERSION ICE NUCLEI. The particles that act as IFN have different surface properties than CCN, and so are left as interstitial particles when cloud droplets are condensing on CCN. These interstitial IFN can experience electroscavenging in clouds below the freezing level, and then act as immersion freezing nuclei when the updrafts lift the droplets above the -15°C level. Again this enhances the formation of ice above the freezing level, affecting cloud and storm dynamics and cloud cover.

- More speculative pathways involve ION-MEDIATED NUCLEATION of ultrafine particles, e.g., in space charge with volatiles released from evaporating droplets at cloud boundaries. ELECTRO-ANTI-SCAVENGING may protect the ultrafine nuclei as they grow into CCN.

Accumulation of charge in cyclonic clouds from uplift of near-surface charged oceanic aerosol subsequently modifies droplet size distributions in later cloud formation

After low J_z days

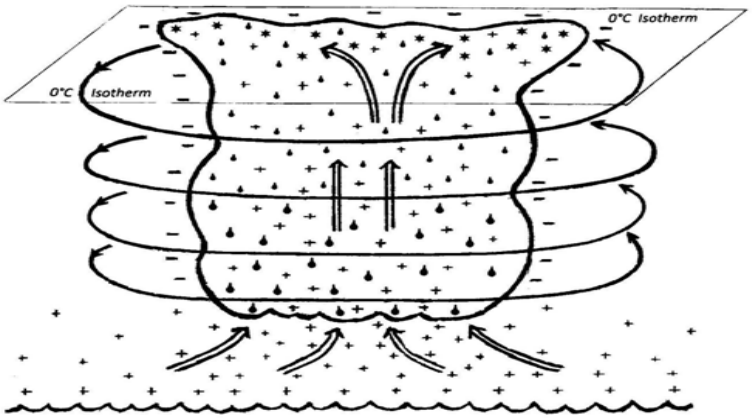

After high J_z days

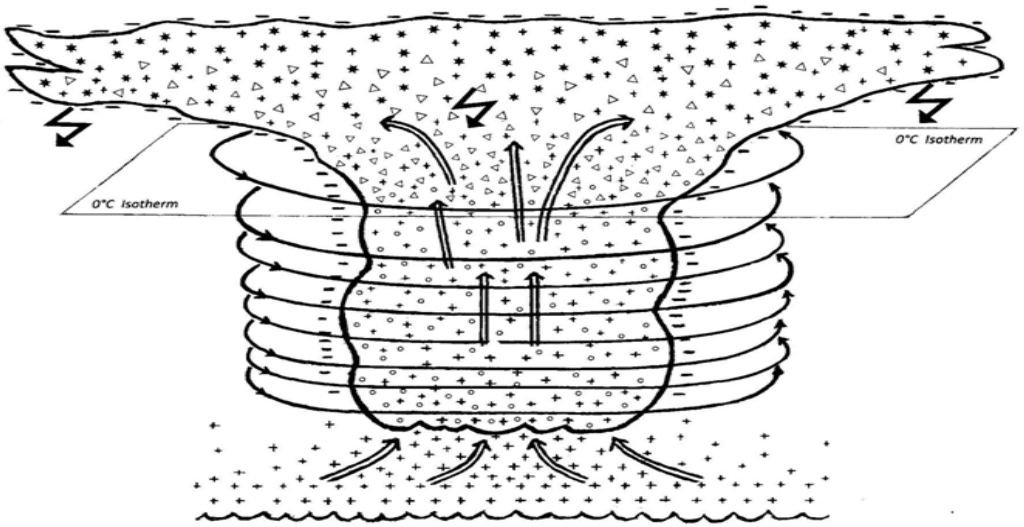

Subsequent to a high J_z day, cloud formation with the J_z–modulated CCN and droplet size distributions gives reduced initial production of rain. More liquid water is carried above the freezing level and releases latent heat of freezing, which invigorates the updrafts (Rosenfeld et al., 2008).

The strengthened updraft increases the vorticity, giving correlations of winter cyclone vorticity with J_z, as observed.

The extra ice is also consistent with greater average winter lightning observed for greater GCR flux in 1990-2005, and less lightning following Forbush decreases (Chronis, 2009).

APPLICATION OF RESULTS OF CLOUD MODELS TO GLOBAL CIRCULATION MODELS

- The microphysical pathways discussed involve changes in drop size distributions, ice production, latent heat release, cloud cover, and the dynamics of storms.

- The radiation budget of a region is affected by changes in cloud cover ; the difference between cooling due to backscattering solar shortwave radiation and warming due to trapping the infrared and re-radiating it down.

- Changes in storm dynamics as well as radiation budget affect the general circulation, and the amplitude of Rossby waves that appear in the jet stream. Prolonged changes in circulation give rise to changes in regional/seasonal climate.

- The application to GCMs will be the final stage of modeling when there are reliable models of cloud charging and the electrical effects on microphysics.

Summary and Conclusions

- There is strong evidence for atmospheric dynamical responses to current density (Jz) changes in the global electric circuit.
- It is consistent with a mechanism involving electrical charging of clouds causing changes in cloud microphysics.
- There is also evidence of changes in cloud cover, either as a direct result of microphysical changes, or an indirect result of dynamical changes. This uncertainty could be resolved by analysis of response times.
- There is uncertainty in initial charging of cyclonic clouds, which could be resolved by in situ observations (by UAVs?) compared to observations of J_z near the clouds (again by UAVs?) and by modeling.
- There are uncertainties about which detailed microphysical pathways are most important. These could be resolved by modeling and in-situ measurements.
- There is a need to model stratospheric and mesospheric conductivity and composition during periods with and without volcanic aerosols , and during solar and magnetic quiet times in comparison to times of MeV electron precipitation.

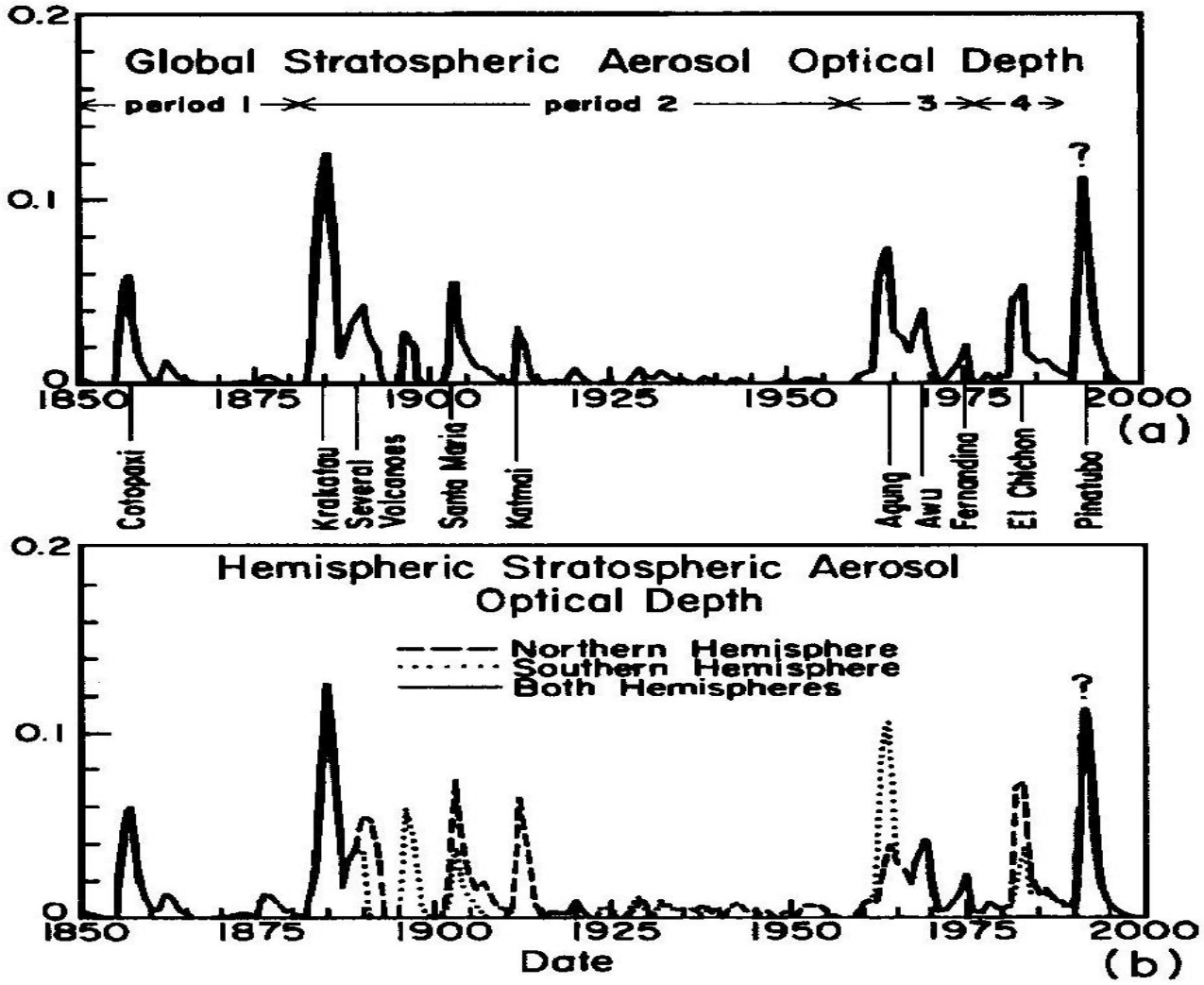

Fig. 1. Estimated stratospheric aerosol optical depth at $\lambda = 0.55$ μm: (*a*) global mean and (*b*) hemispheric means.

Stratospheric optical depths, based on extinction measurements, satellite occultation measurements, and other proxy data. (Preliminary data for Pinatubo). From Sato et al., (1993).

From Meyerott et al., p.449 – 460, in Weather and Climate Responses to Solar Variations. Colo. Ass. Univ. Press. 1983

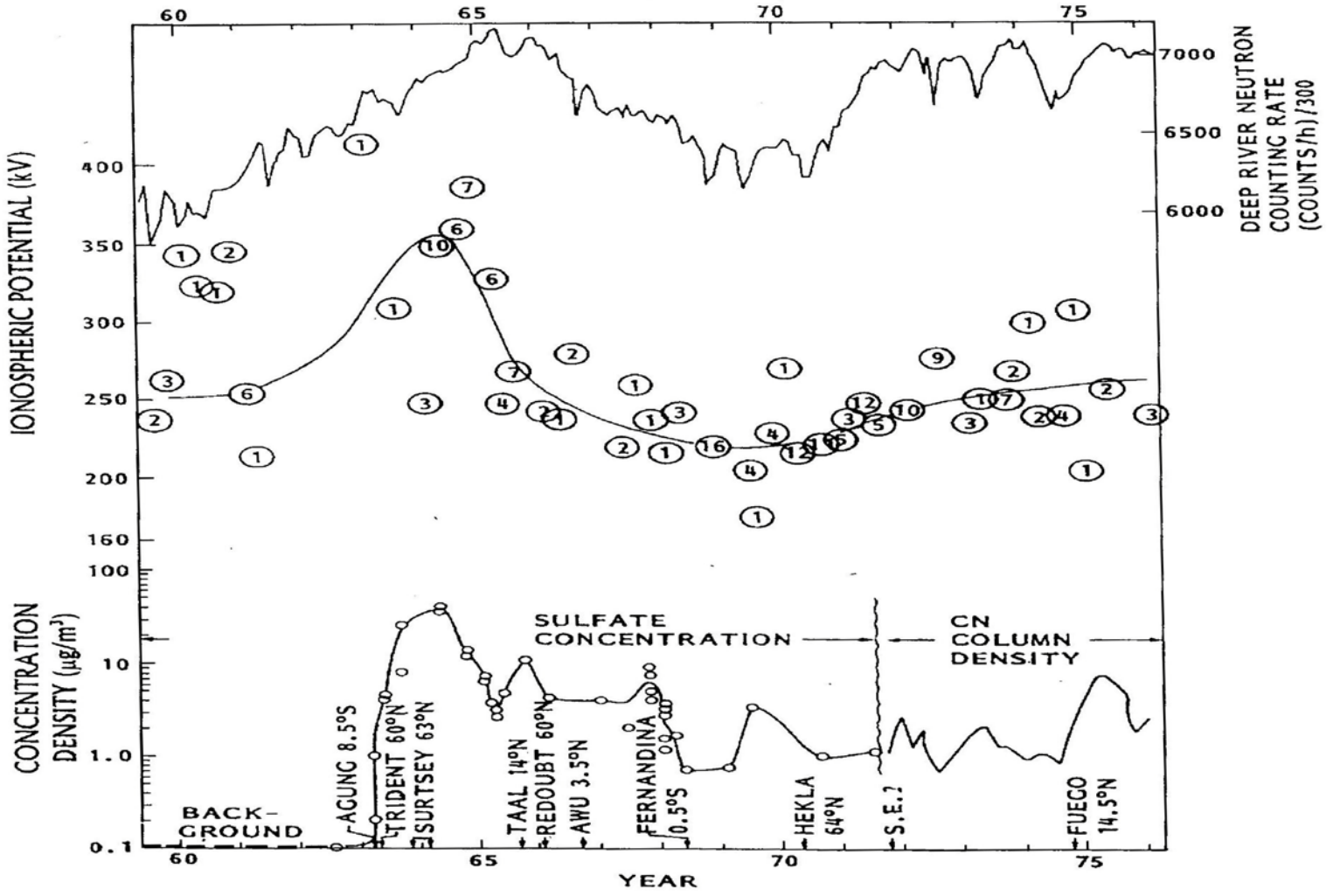

GCR flux (top), 12 km potential from Mühleisen and Fischer (middle), and stratospheric aerosol content (bottom), 1959-1976

REDISTRIBUTION AND PERSISTENCE OF H_2SO_4 IN STRATOSPHERE

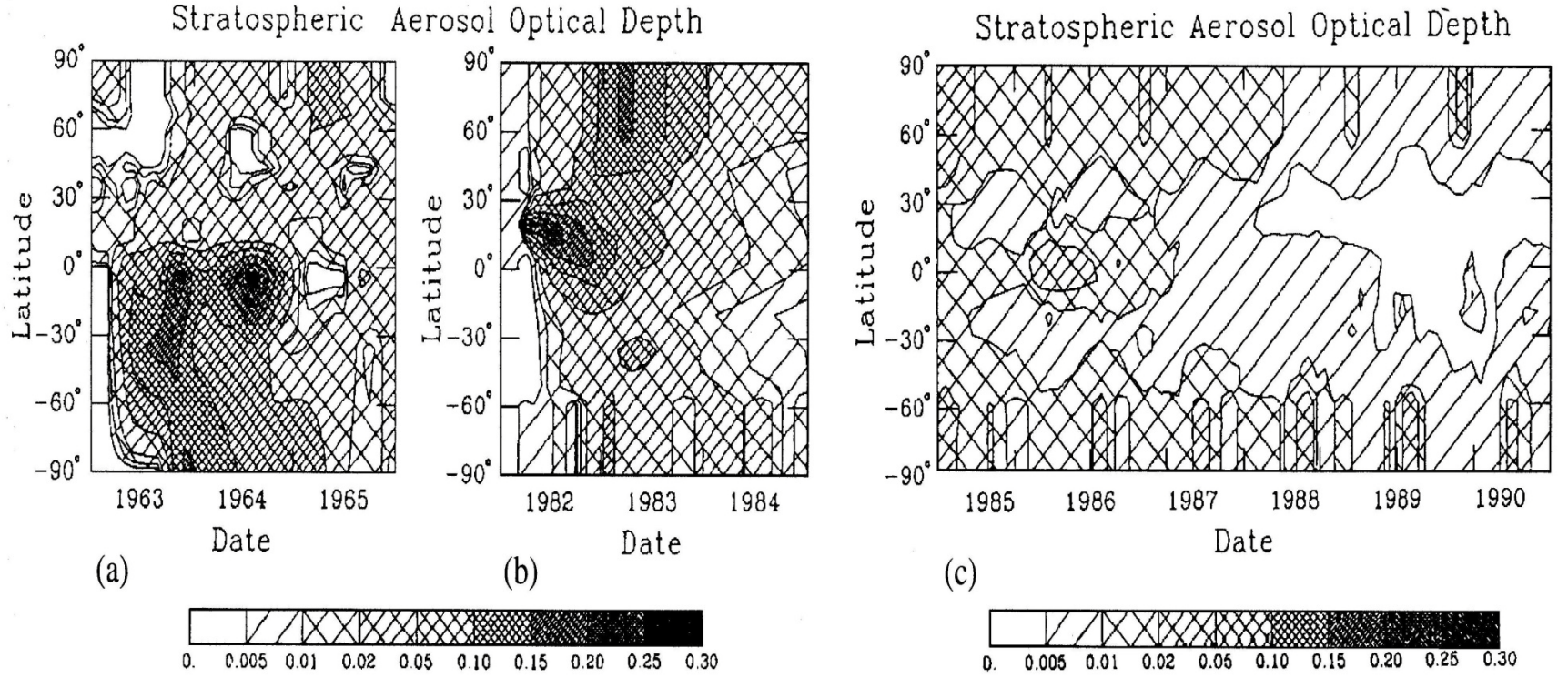

Fig. 5. Estimated stratospheric optical depth at $\lambda = 0.55$ μm as a function of latitude and time; (a) period after Agung; (b) period after El Chicon; (c) period from 1985 to 1990. From Sato et al. (1993).

The H_2SO_4 is formed from volcanic SO_2 and is transported by the Brewer-Dobson circulation. Larger aerosol particles appear 5-10 km above the tropopause, and become concentrated in the winter at higher latitudes than □60 . (Sato et al., (1993).

H. J. Fischer and R. Mühleisen, “The ionospheric potential and the solar magnetic sector boundary crossings”, Report Astronomisches Institut der Universität Tübingen, 1980.

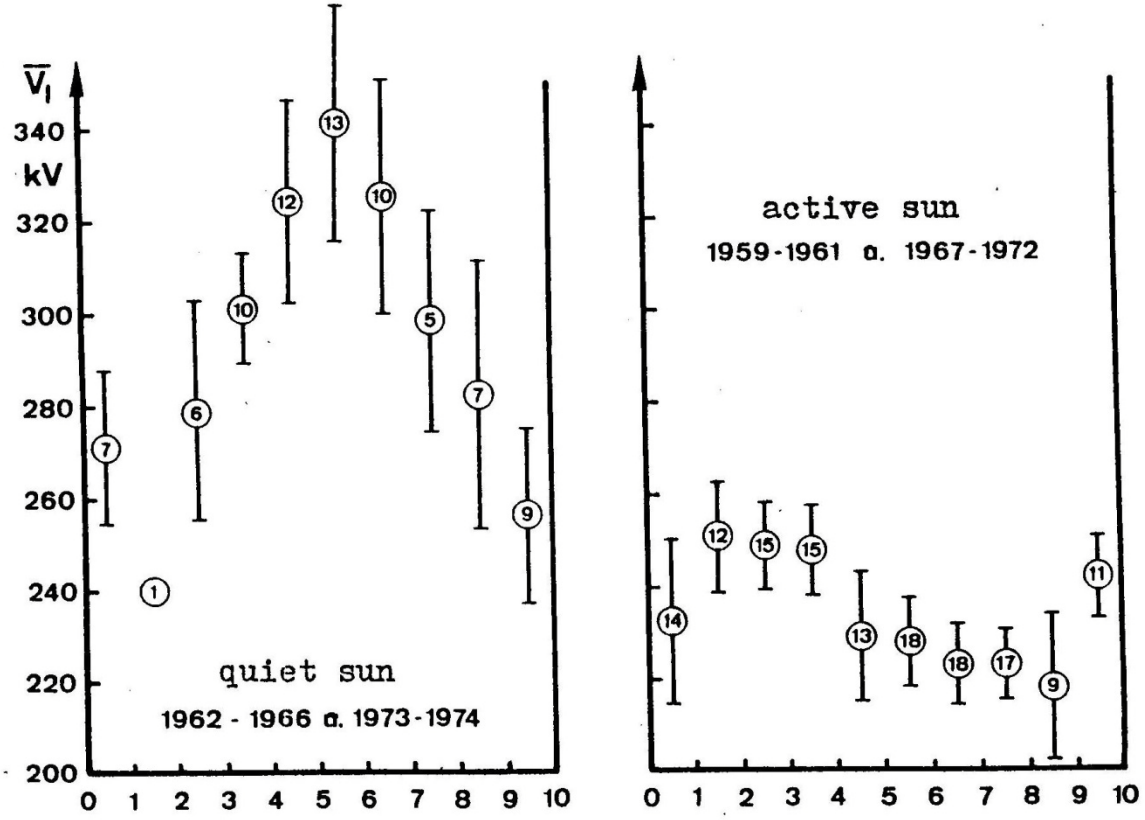

Potential from balloon soundings to 12 km, from southern Germany, sorted by position in solar wind magnetic sectors. Sector boundaries are 0 and 10.

From Reiter, J. Atmos. Terr. Phys., 39, 95-99, 1977.

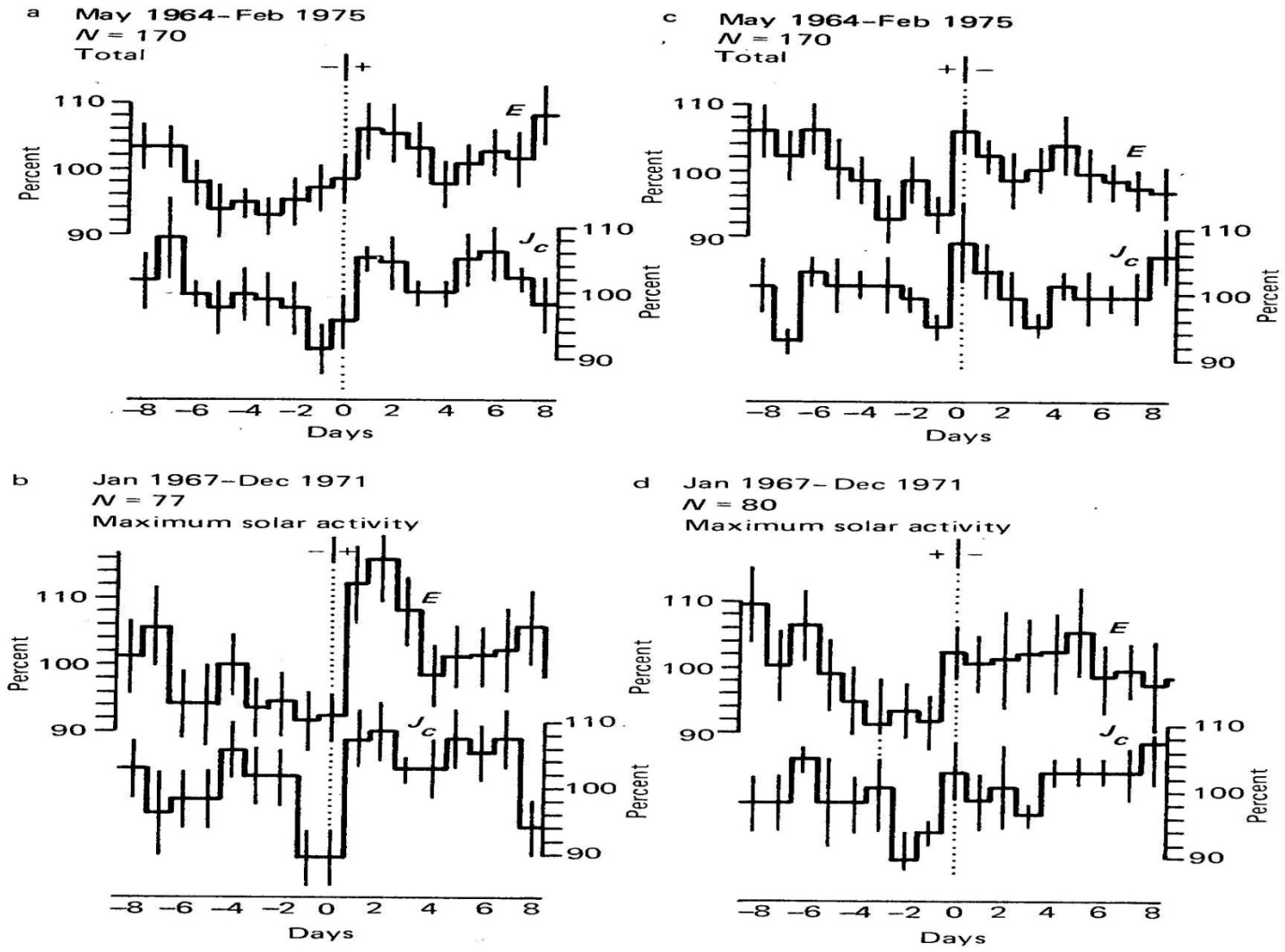

Superposed epochs for electric field (E) and current density (J) measured at Zugspitze, with key days those of either -/+ or +/- solar wind sector boundary crossings.

Surface vertical field compared to overhead ionospheric potential from satellite observations: day zero is IMF B_y polarity change

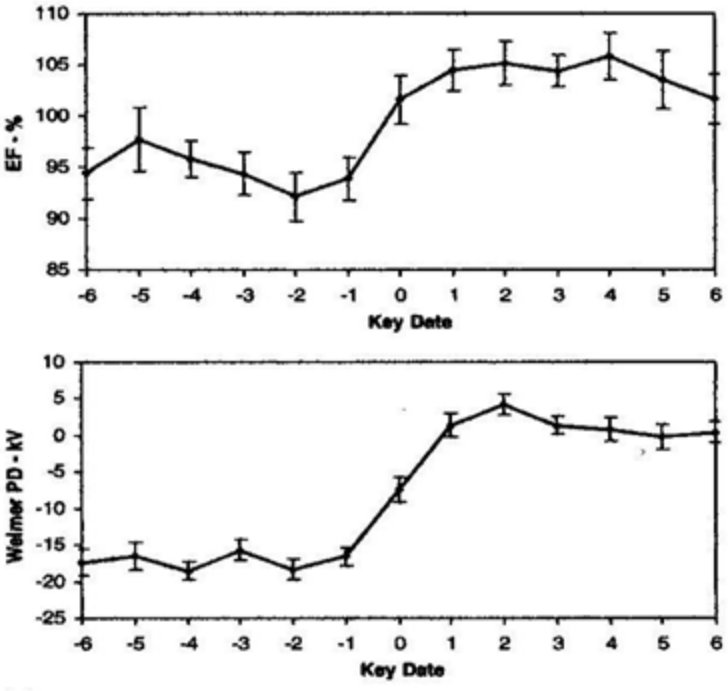

Left Panels: Vostok surface electric field (top) and ionospheric potential (bottom) for ‘toward-to-away’ HCS crossings. Average of 30 crossings. Burns et al., (2006)

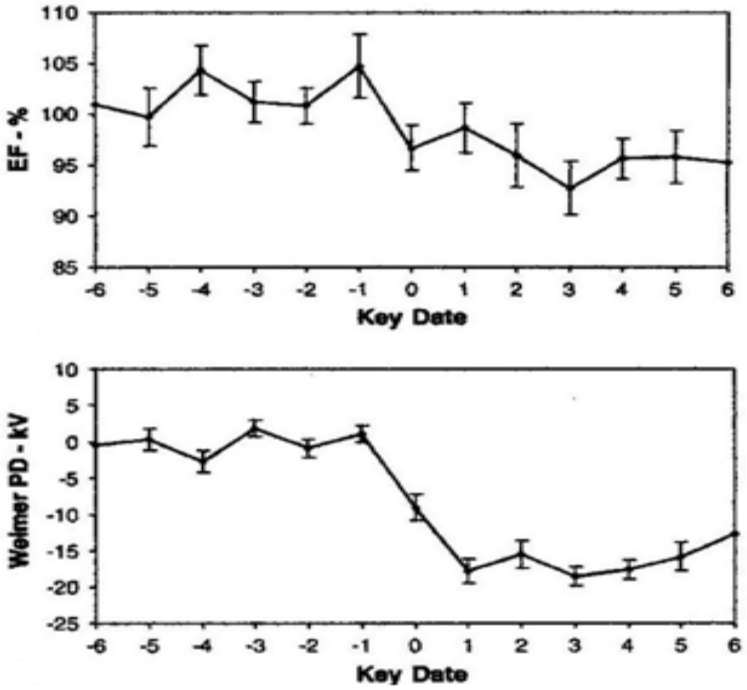

Right Panels: Vostok surface electric field (top) and ionospheric potential (bottom) for ‘away-to-toward’ HCS crossings. Average of 23 crossings. (Burns et al. (2006).

THE SOLAR WIND ELECTRIC FIELD ENTERING THE ATMOSPHERE VIA THE POLAR IONOSPHERES

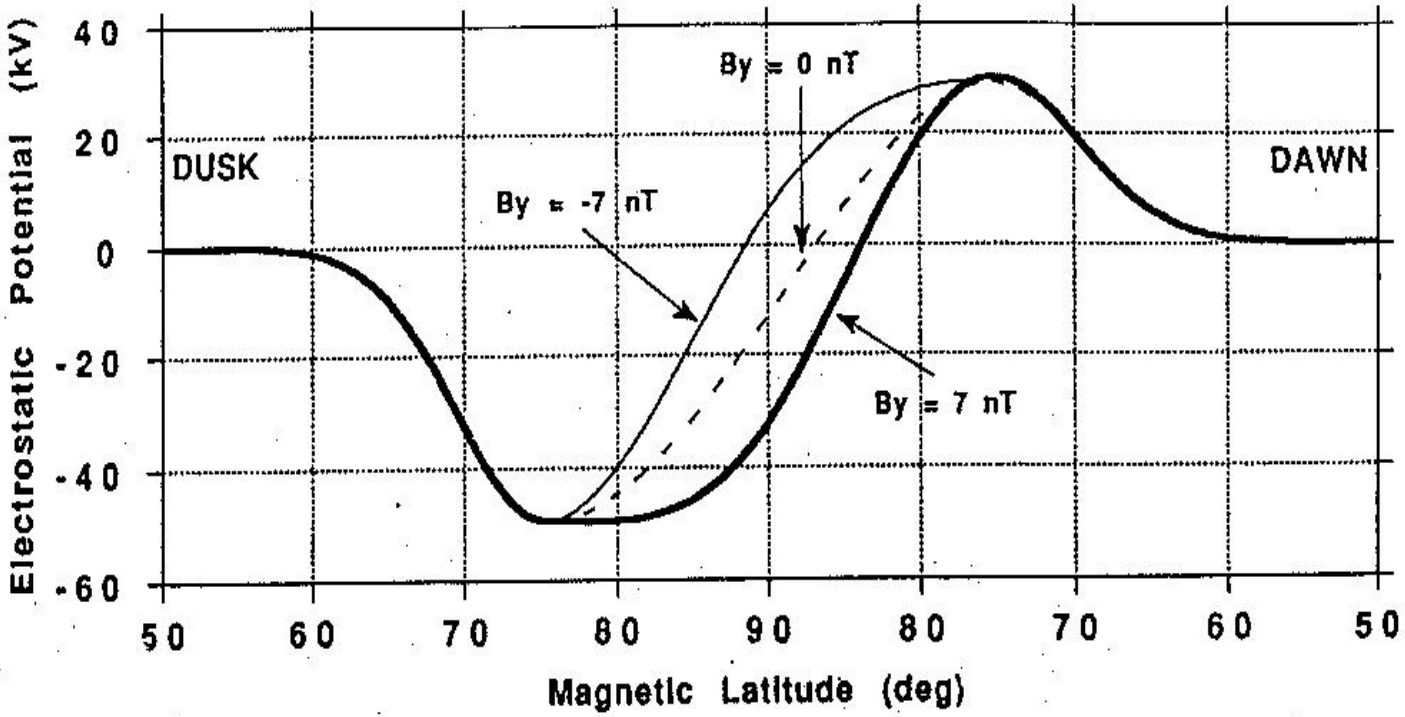

The solar wind (VxB) electric field is mapped down magnetic field lines at magnetic latitudes greater than about 60^o. The B_z component gives the dawn and dusk electric field excursions (V_xx B_z) that appear as ionospheric potential changes, maximizing near 75^o magnetic latitude. The B_y component gives a north south electric field excursion (V_xx B_y) that appears as an ionospheric potential variation that maximizes at the magnetic poles

All the excursions of ionospheric potential are superimposed on a ~250 kV potential difference between the ionosphere and the earth's surface generated by thunderstorms.

Right: Regressions of daily-average Weimer-2001 ionospheric potential at polar locations against the IMF B_Y.

Left: Regressions of daily-averaged surface pressure at the same polar sites

Data splits are:

1995 to 2005 Antarctic

(mlat>83º;

mlat~81º;

mlat<75º)

and 1999 to 2002 Arctic (mlat>83º).

Error bars are plus/minus one standard-error-in-the mean

(Burns et al., JGR, *113*, D15112, 2008)

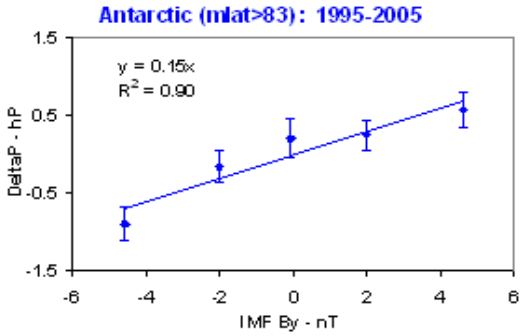

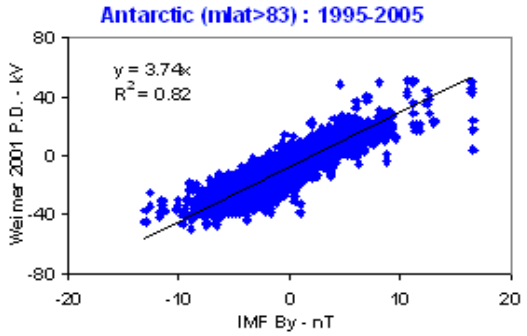

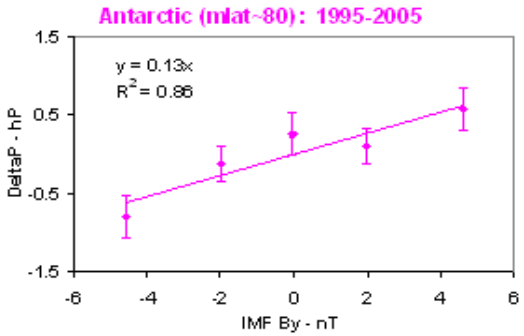

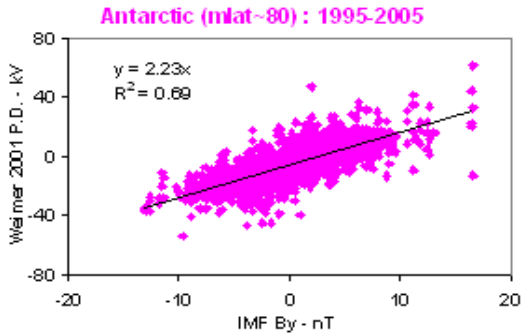

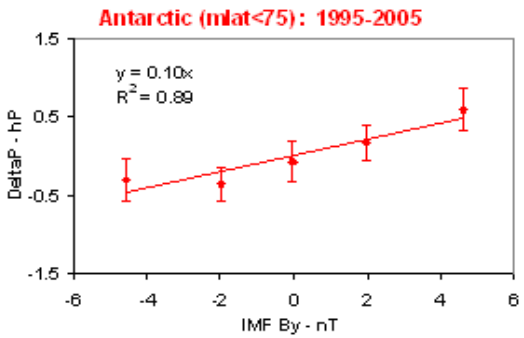

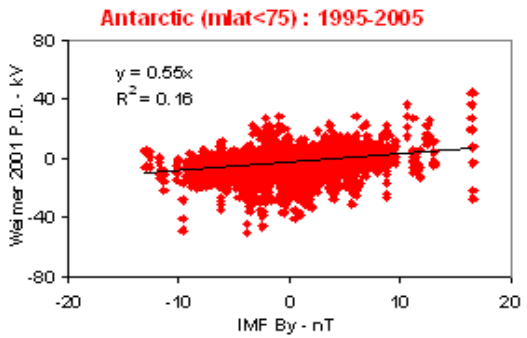

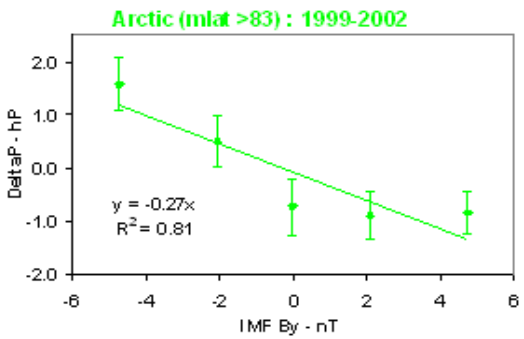

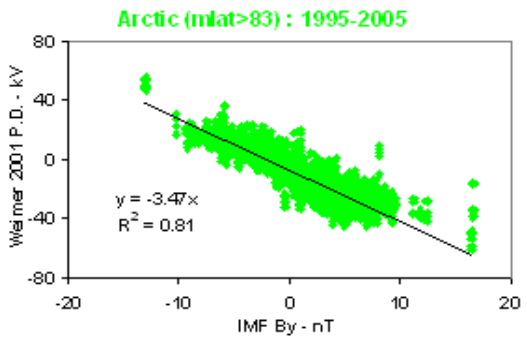

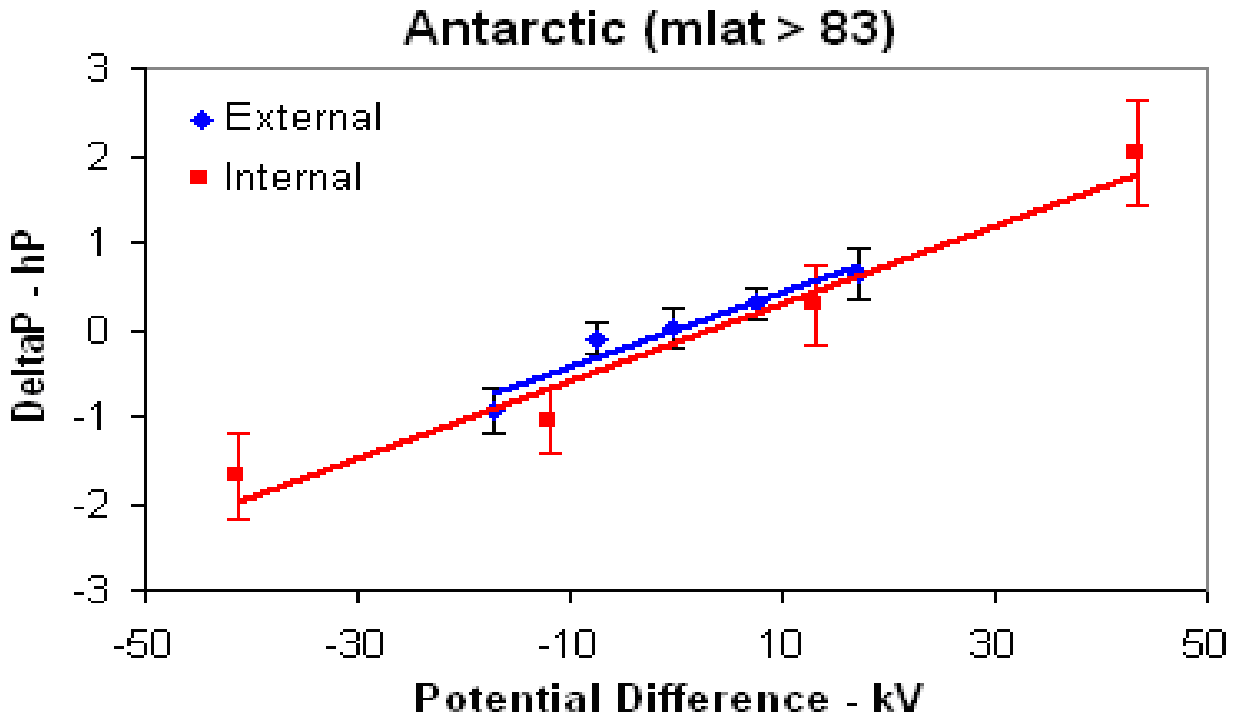

Pressure variations for the Antarctic magnetic latitude > 83 region, associated with internal (thundercloud generators - red) and external (solar wind electric field - blue) inputs to the global circuit.

(The drivers have been converted to their respective associated ionospheric potential changes using Weimer (2001) for the external driver, and a mean ionospheric potential of 240 kV for the internal driver.) From Burns et al., *JGR 113,* D15112 (2008).

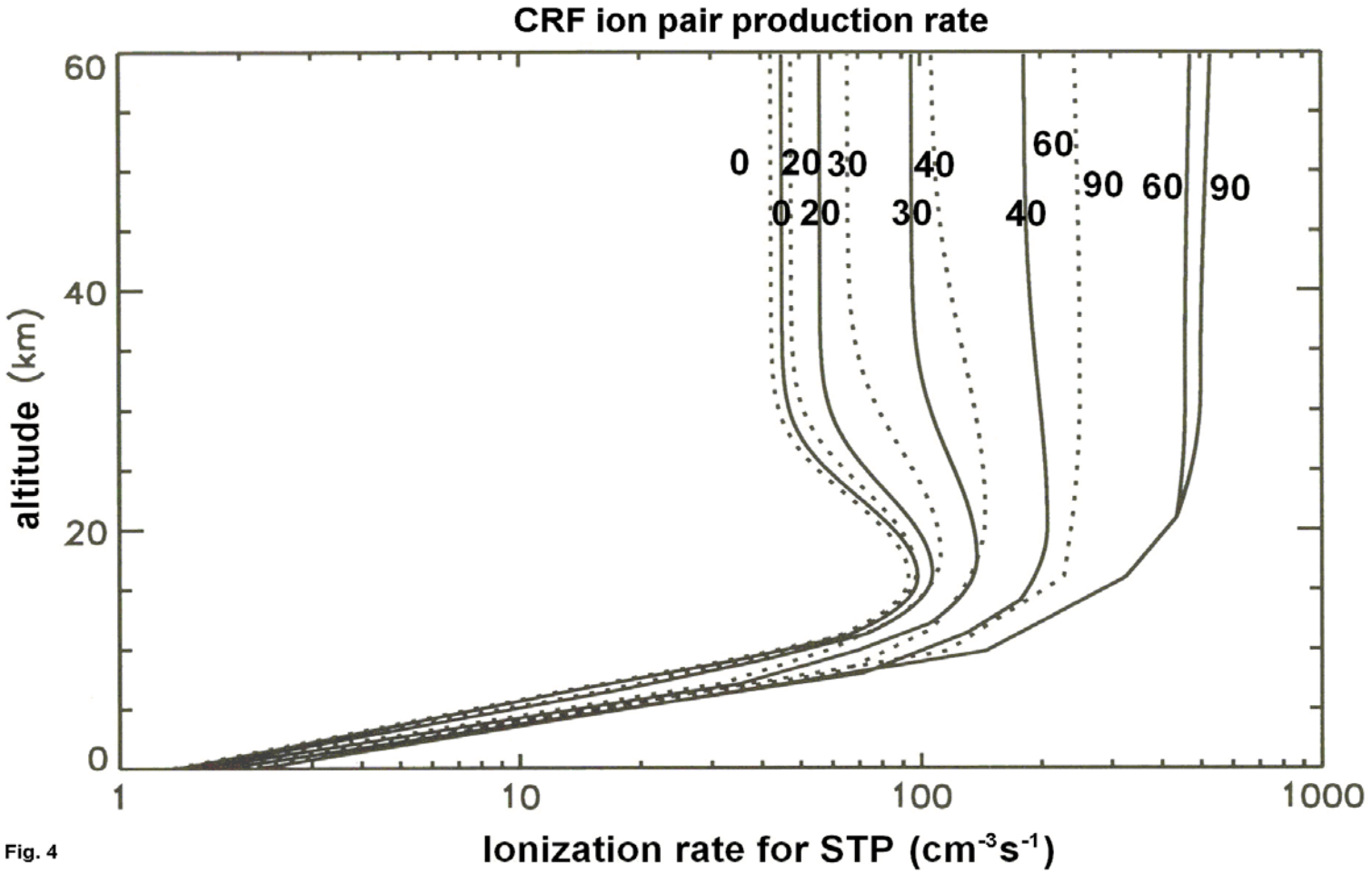

Fig. 4

Variation in ion-pair production rate from GCR for air at STP (i.e., per mass unit), as a function of altitude for gm-latitudes 0 , 20 , 40 , 60 , and 90 . The solid lines are for solar minimum, and the dashed lines for solar maximum. From Tinsley and Zhou, (2006)

DISTRIBUTION OF COLUMN RESISTANCE OVER THE GLOBE

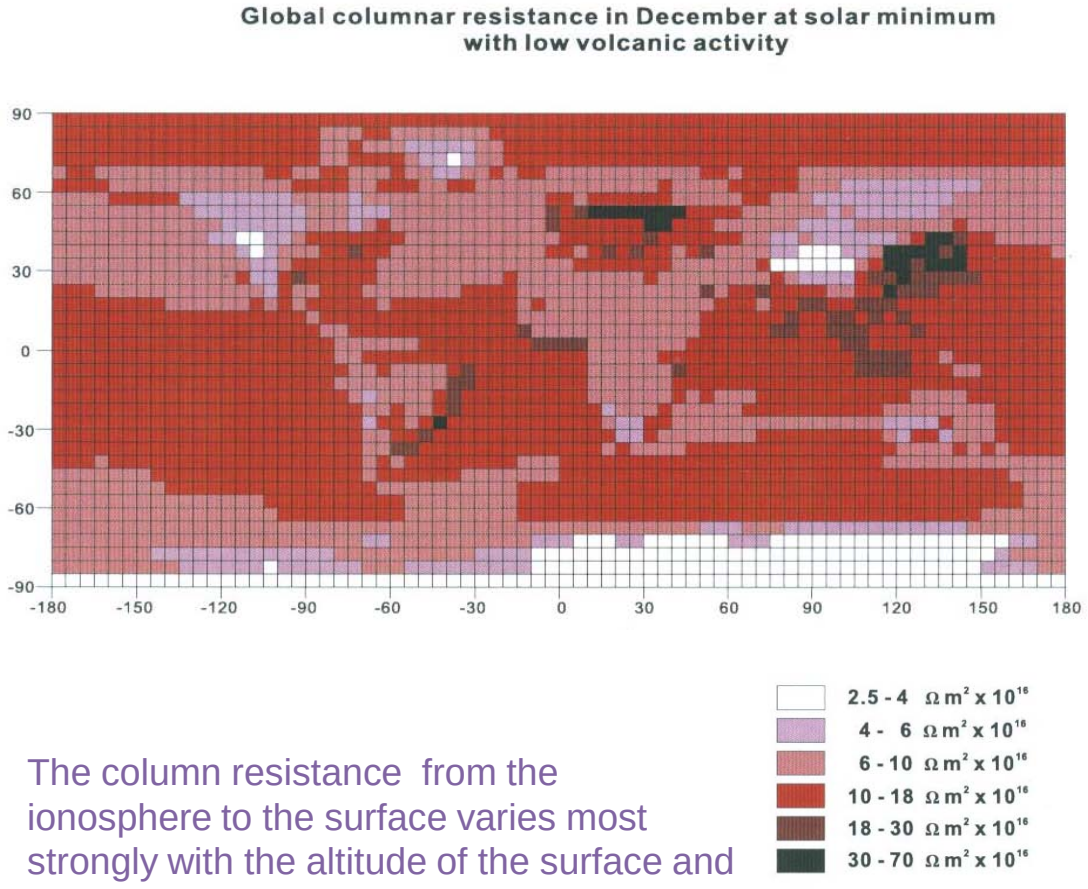

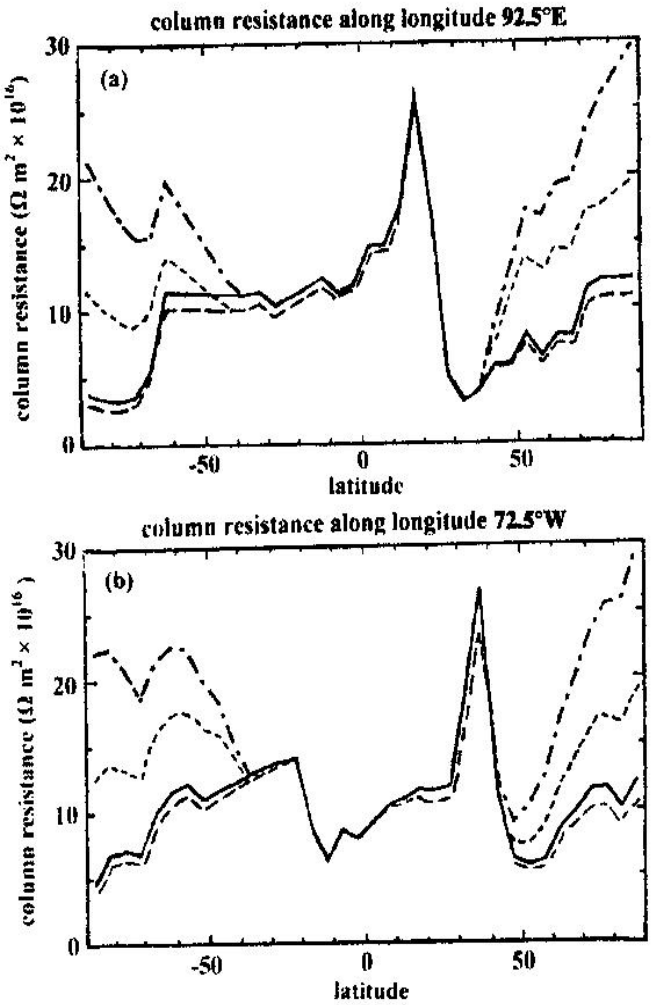

The column resistance from the ionosphere to the surface varies most strongly with the altitude of the surface and the aerosol content of the troposphere and stratosphere. The column resistance is least over mountains and Antarctica and Greenland, and greatest in industrial areas that generate high aerosol loadings.

Solid curves are for solar maximum and large dashed curves for solar minimum in absence of stratospheric ultrafine aerosols. Dot-dash curves for solar max. and small dashed curves for solar min. with stratospheric aerosols.

GLOBAL CIRCUIT COLUMN RESISTANCE VARIATION WITH SOLAR CYCLE (AND FORBUSH DECREASE) OF COSMIC RAY FLUX

Columnar resistance variation percentage from solar minimum to solar maximum in December with low volcanic activity (a)

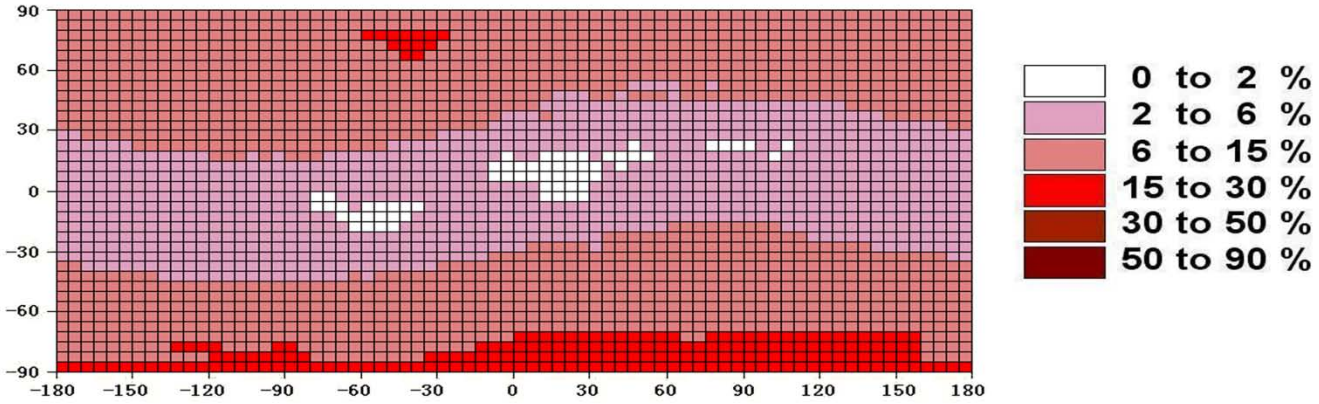

Columnar resistance variation percentage from solar minimum to solar maximum in December with high volcanic activity (b)

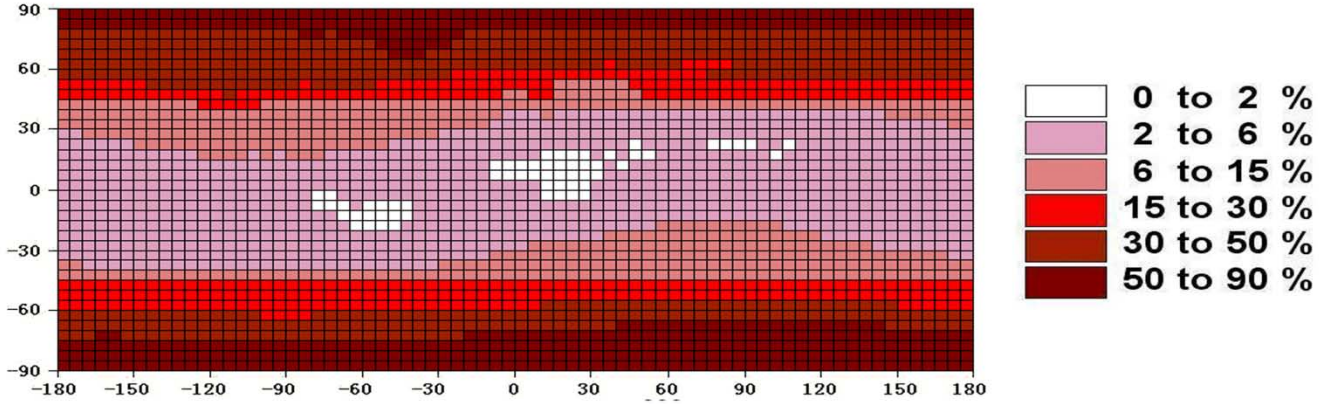

Mean Absolute Electric Charge on Cloud Droplets and Raindrops

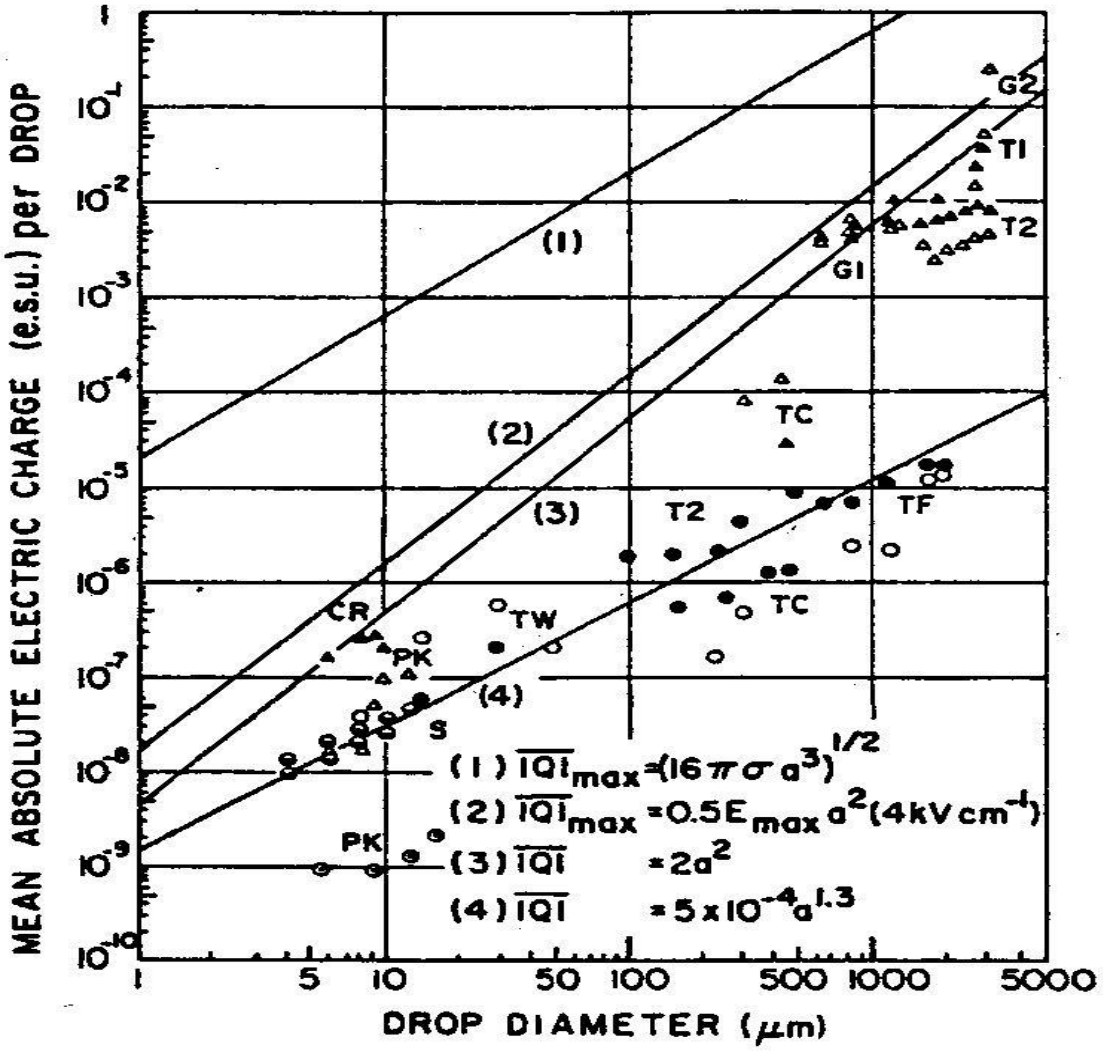

Round symbols for warm cloud cases; triangular for thunderstorms. From Takahashi (1973) and Pruppacher and Klett (1997). 4.8×10^{-10} e.s.u. = 1e

PRODUCTION OF SPACE CHARGE BY CURRENT FLOW (J_z) THROUGH A GRADIENT OF CONDUCTIVITY DUE TO AERSOLS

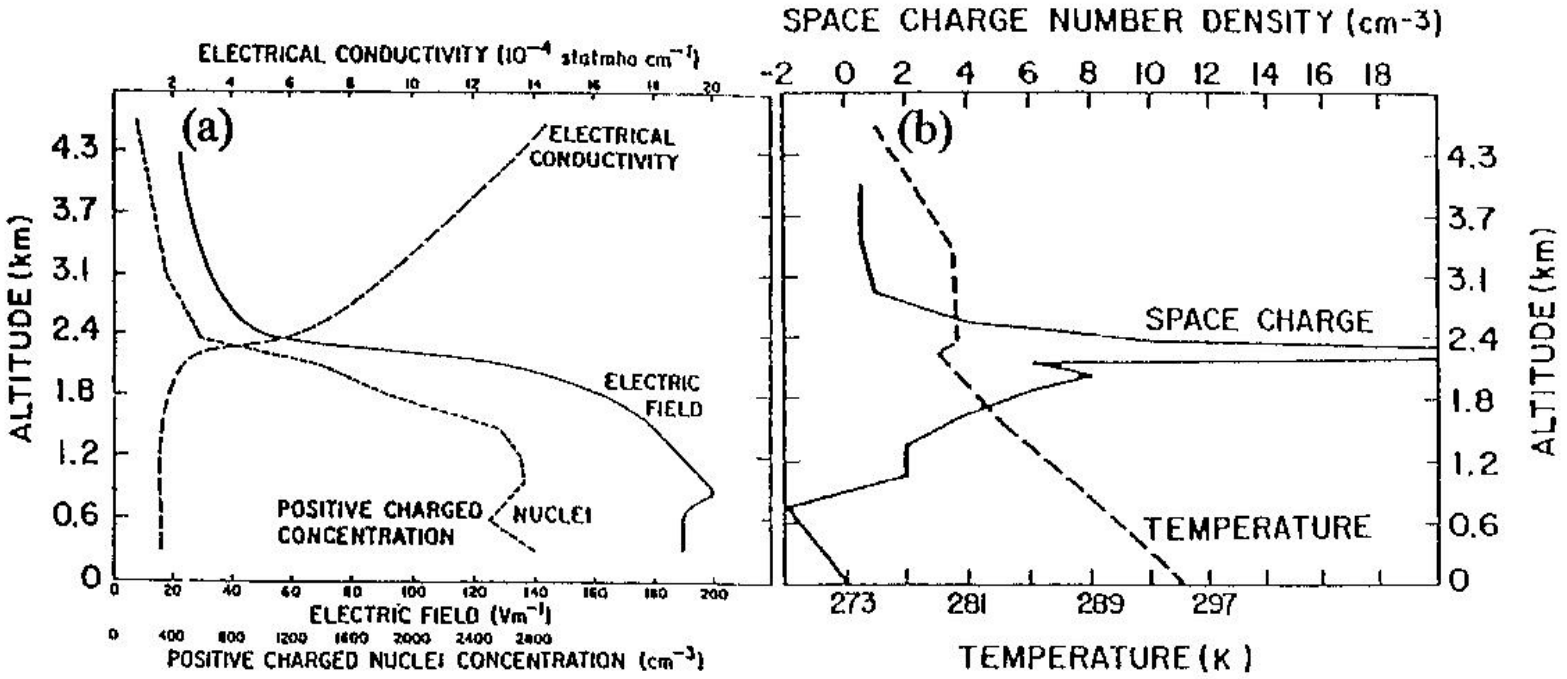

(a) Measurements made in mid afternoon in the north-eastern USA from an aircraft on 20 August 1953, with the top of the mixing layer (boundary layer) in the lower troposphere at 2.2 km altitude. The high aerosol concentration produces a low conductivity and high concentrations of positive (and negative) charged aerosol particles. With constant vertical current density J_z the electric field E increases (Ohm's Law, $E = J_z/\sigma$).

(b) Calculations show the presence of space charge (ρ) in the gradient of electric field near the top of the mixing layer (Gauss's Law, $dE/dz = \rho/\varepsilon_o$). From Sagalyn and Faucher, 1954.